Geol. Mag. **151** (*4*), *2014, pp. 573–590.* © *Cambridge University Press 2013*
doi:10.1017/S0016756813000551

Source character, mixing, fractionation and alkali metasomatism in Palaeoproterozoic greenstone dykes, Dannemora area, NE Bergslagen region, Sweden

PETER DAHLIN*†, ÅKE JOHANSSON‡ & ULF B. ANDERSSON*§

*Department of Earth Sciences, Uppsala University, Villavägen 16, SE-75236 Uppsala, Sweden
‡Laboratory for Isotope Geology, Swedish Museum of Natural History, Box 50 007, SE-10405 Stockholm, Sweden
§LKAB, Research and Development, TFG, SE-981 36 Kiruna, Sweden

(*Received* 21 November 2012; *accepted* 19 June 2013; *first published online* 13 August 2013)

Abstract – The geochemical and isotopic characteristics of metamorphosed Svecofennian mafic dykes from the Dannemora area in the NE part of the Bergslagen region in central Sweden were investigated and compared to mafic intrusive rocks in their vicinity. The dykes, with an inferred age of *c.* 1860–1870 Ma, are calc-alkaline, sub-alkaline and basaltic in composition and have a mixed subduction and within-plate geochemical affinity. They are the result of mixing of at least three mantle source components with similar basaltic major element composition, but different concentrations of incompatible trace elements. Magma M1 is strongly enriched both in Rare Earth Elements (REE) and High-Field-Strength Elements (HFSE); magma M2 is highly enriched in Large-Ion Lithophile Elements (LILE, except Sr) with only moderate enrichment in HFSE and REE (particularly low in Heavy Rare Earth Elements); and magma M3 is enriched in Sr and has a flat REE profile. Magma M3 also has a somewhat more positive (depleted) initial ε_{Nd} value of +1.8, compared to +0.4 to +0.5 for magmas M1 and M2. The magma evolution was controlled by a mixture of fractionation (mainly affecting the compatible elements) and mixing, best seen in the incompatible element concentrations and the Nd isotope data. The basaltic overall composition indicates little or no wholesale contamination by upper continental crust, but the dykes have undergone later metasomatic changes mainly affecting the alkali elements.

Keywords: Svecofennian, Bergslagen region, Dannemora, greenstone dykes, alkali metasomatism

1 Introduction

Mafic rocks are important messengers from the mantle, and their geochemistry may provide crucial information about mantle composition, magma generation and tectonic processes during their formation. In a couple of recent papers, the geochemistry of *c.* 1.9 Ga old ultrabasic and basic rocks within the Palaeoproterozoic Svecofennian orogen of the Fennoscandian Shield in east-central Sweden has been discussed (Johansson *et al.* 2012; Johansson & Hålenius, 2013). Here, we investigate metamorphosed mafic dykes from the Dannemora area in order to assess their formation and compare them with adjacent mafic plutonic rocks. We use major and trace element geochemistry, as well as isotopic signatures of Sr and Nd, in order to decipher their origin, magmatic evolution and tectonic setting and to obtain an insight into Palaeoproterozoic mantle processes and compositions.

2 Geological setting

The Fennoscandian Shield shows a general decrease in age from an Archaean nucleus in the northeast through Palaeoproterozoic rocks in the central part to Meso- and early Neoproterozoic rocks in the southwest (e.g. Gaál & Gorbatschev, 1987). The Palaeoproterozoic Svecofennian orogen covers the central part of the shield. It is succeeded by the Transscandinavian Igneous Belt (TIB) to the southwest, and overlain by Caledonian nappes to the west and northwest (Fig. 1). The evolution of the Svecofennian orogeny has been divided into four stages: the formation and accretion of microcontinents and volcanic arcs; extension of the newly formed crust; continent–continent collision and crustal thickening; and finally gravitational collapse (e.g. Nironen, 1997; Lahtinen *et al.* 2005; Korja *et al.* 2006). The entire tectonic evolution roughly spans 1.92–1.77 Ga (e.g. Lahtinen *et al.* 2005), with the various stages partly overlapping in space and time (e.g. Andersson *et al.* 2004*b*; Korja *et al.* 2006; Rutanen & Andersson, 2009). Hermansson *et al.* (2008) proposed a model in which the evolution of the central part of the orogen is the result of migratory tectonic switching of extension and compression within the overriding plate as a response to subduction hinge migration.

The Bergslagen region, which is located in the south-central part of Sweden (Fig. 1), constitutes the southern part of the Svecofennian orogen. The region is dominated by plutonic rocks and subordinate supracrustal rocks (e.g. Stephens *et al.* 2009), the latter containing

†Author for correspondence: peter.dahlin@geo.uu.se

https://doi.org/10.1017/S0016756813000551 Published online by Cambridge University Press

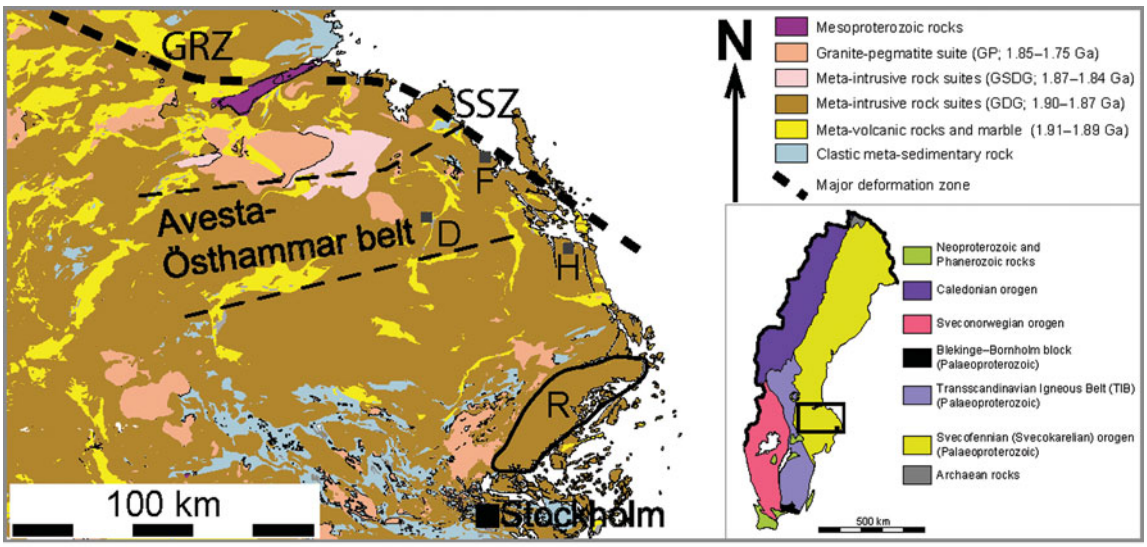

Figure 1. (Colour online) Map of the geology of the northern Bergslagen region after Stephens *et al.* (2007). The region is dominated by rocks of the granite-diorite-gabbro (GDG) suite and subordinate metavolcanic rocks. The southern part consists mainly of clastic metasedimentary rocks and anatectic granites. Locations: D – Dannemora area (Fig. 2); F – Forsmark; H – Herräng; R – Rådmansö and the southern Roslagen gabbro area. Regional deformation zones: GRZ – Gävle–Rättvik Zone; SSZ – Singö Shear Zone. Inset (right) shows geological provinces of Sweden with the northern Bergslagen region marked.

both base metal sulphide and iron oxide deposits (e.g. Allen *et al.* 1996; Stephens *et al.* 2009).

The Bergslagen region is bounded by the Gävle–Rättvik zone (GRZ in Fig. 1; Högdahl *et al.* 2009) and Singö shear zone (SSZ in Fig. 1; Tirén & Beckholmen, 1990) to the north and by the TIB (Högdahl *et al.* 2004) to the south. The GRZ coincides with a metamorphic break with higher-grade partly migmatized rocks to the north and greenschist- to amphibolite-grade rocks to the south (Stålhös, 1991; Andersson, 2005). These tectonic zones have been suggested to represent terrane boundaries or crustal-scale domain boundaries (Lahtinen *et al.* 2005; Högdahl *et al.* 2009) or separate tectonic domains (ductile high-strain belts; Hermansson *et al.* 2007).

The Bergslagen region itself has been interpreted as a rifted continent (e.g. Oen *et al.* 1982; Van der Velden *et al.* 1982), a microcontinent (Lahtinen *et al.* 2005; Beunk & Kuipers, 2012) or a back-arc region similar to the present Taupo Volcanic zone in New Zealand (Allen *et al.* 1996). The central part of the region chiefly consists of migmatized metasediments, and metagranitoids with related anatectic granites (Stephens *et al.* 2009). Metavolcanic rocks occur in subordinate amounts as narrow inliers, with U–Pb zircon ages ranging between 1.91 and 1.89 Ga (e.g. Andersson *et al.* 2006*a*; Lundström *et al.* 1998; Stephens *et al.* 2009, and references therein). Partly coeval with the metavolcanic rocks are the 1.90–1.87 Ga meta-intrusive rocks of the granite-diorite-gabbro (GDG) suite (Stephens *et al.* 2009). Younger groups of plutonic rocks are the 1.87–1.84 Ga granite-syenite-diorite-gabbro (GSDG) intrusive rock association and the mainly undeformed 1.85–1.75 Ga granite-pegmatite (GP) suite (Stephens *et al.* 2009).

The metamorphic grade in the Bergslagen region is mainly amphibolite facies with isolated areas of greenschist facies in the western parts and granulite facies in the south (Stephens *et al.* 2009). Two major metamorphic peaks at *c.* 1.87 and 1.80 Ga have been recognized from U–Pb dating of zircon and monazite (e.g. Andersson *et al.* 2006*a*; Hermansson *et al.* 2008). The region experienced poly-deformation with two or locally three fold phases that formed during peak metamorphic conditions (Persson & Sjöström, 2003; Stephens *et al.* 2009).

2.a Mafic dykes in the Bergslagen region

Mafic and ultra-mafic intrusive bodies are scattered in the Bergslagen region (e.g. Stålhös, 1991; Stephens *et al.* 2009; Rutanen & Andersson, 2009; Johansson *et al.* 2012; Johansson & Hålenius, 2013). Mafic dykes are very common, and Stålhös (1991) divided them into three generations. The first generation occurs as mafic dykes in the oldest supracrustal and as enclaves in the GDG suite and is interpreted as syn-magmatic with the granitoids (Andersson, 1991; Wikström, 1992), possibly representing feeder dykes to supracrustal basalts (Stålhös, 1991; Stephens *et al.* 2009). Dating of a metaaplite, co-magmatic with the mafic and granitoid host rock (first dyke generation) at Forsmark (F in Fig. 1), gave a U–Pb zircon age of 1891 ± 13 Ma (Stephens *et al*. 2009). Dating of a metagabbro in the Forsmark area gave a U–Pb (zircon) age of 1886 ± 1 Ma (Hermansson *et al*. 2008).

The second generation, referred to as Herräng dykes (Magnusson, 1940), occurs as abundant WNW–ESE-trending dykes in the NE part of the Bergslagen region, and ranges from dominantly basic to subordinately intermediate and felsic in composition (Stålhös, 1991). These dykes intrude both supracrustal and metaplutonic rocks but are themselves deformed

https://doi.org/10.1017/S0016756813000551 Published online by Cambridge University Press

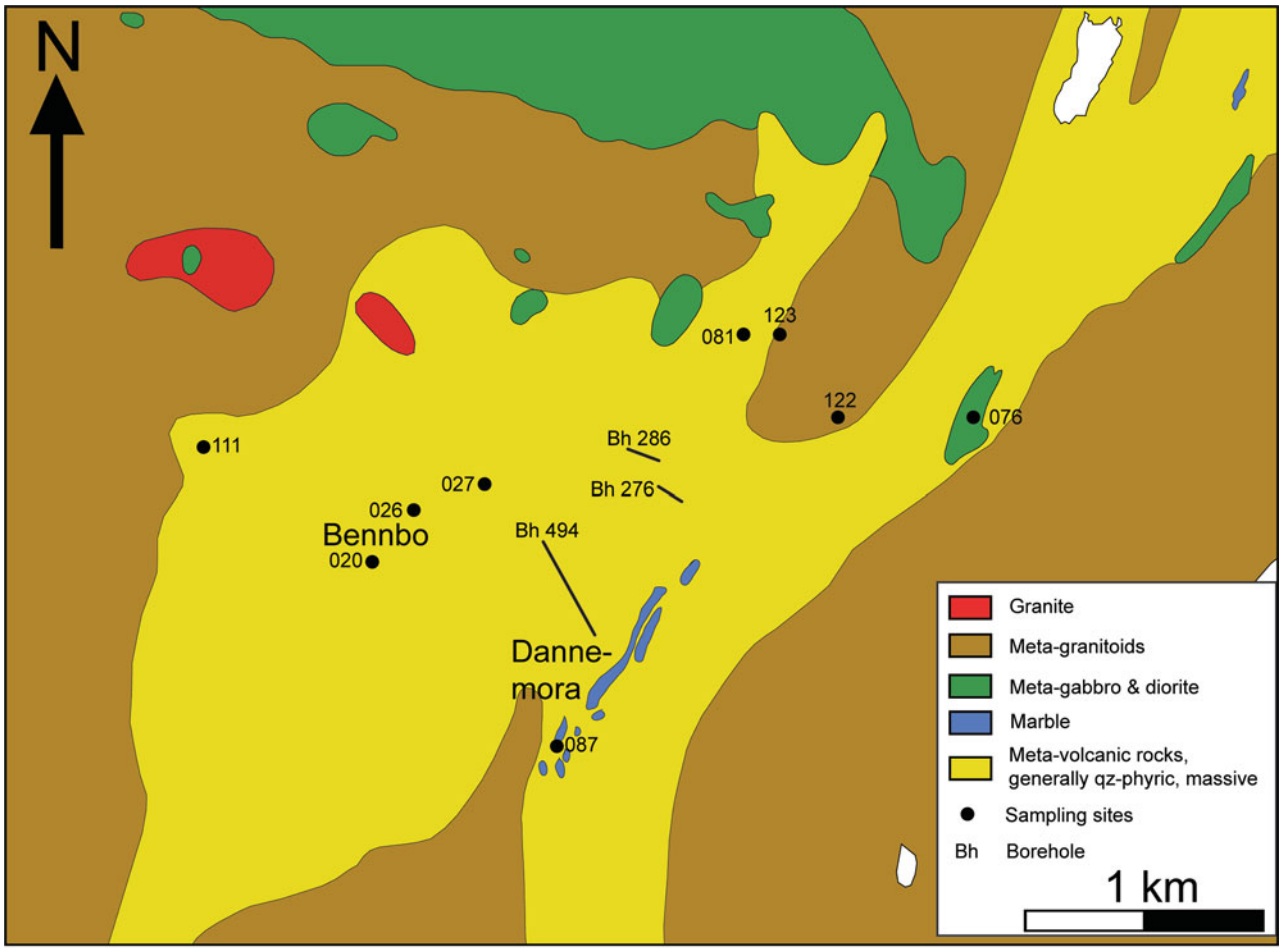

Figure 2. (Colour online) The Dannemora inlier with the GDG-suite that surrounds the slightly older supracrustal rocks and a number of mafic bodies. The sample locations are marked with numbers. Three boreholes (in the central part of the map) were drilled towards the main mining field and cover the whole stratigraphy including the ore horizon (after Stålhös, 1991). © Geological Survey of Sweden (SGU). Dnr: 30–2169/2007.

and metamorphosed, having intruded during an extensional phase followed by renewed compression (cf. Magnusson, 1940; Stålhös, 1991). At Forsmark, dykes belonging to this generation intruded during the time span between 1867 ± 4 Ma (U–Pb zircon age of surrounding granite) and 1859 ± 2 Ma (metamorphic U–Pb titanite age from these dykes; Hermansson *et al*. 2008).

Dykes belonging to the third generation, which actually comprises several individual generations, intruded after the deformation and are very subordinate in the vicinity to Dannemora but abundant in other parts of Bergslagen (e.g. Stålhös, 1991; Risku-Norja, 1992; Andersson, 1997*a*; Söderlund *et al.* 2005).

3 Local geology, sampling and analytical methods

The Dannemora area is located in the NE part of the Bergslagen region (Figs 1, 2). The geology of the area consists of rhyolitic to dacitic metavolcanic rocks and marble, forming a N–S-trending inlier surrounded by metagranitoids (Stålhös, 1991; Lager, 2001; Dahlin *et al*. 2012). Iron oxide ore and subordinate sulphide ore occur within the supracrustal sequence.

Numerous dykes have been recorded in the Dannemora area and the surrounding metagranitoids. Törnebohm (1878) had already described five different dykes ranging from mafic to felsic in composition, mainly based on underground mine mapping in the Dannemora ore field.

For this study, 18 samples of *c.* 1 kg each were collected from an area of 3 × 2 km around Dannemora: 8 dykes from outcrops, 9 dykes from three drill cores and one sample (076) from an outcrop interpreted as basaltic amphibolite by Stålhös (1991). This interpretation could not be confirmed as no contacts were possible to observe; this sample will therefore be treated as the others but highlighted with a different symbol in the diagrams. The sample strategy was to cover as large an area and as many types of host rock as possible i.e. marble, metavolcanics and metagranitoids. Table 1 displays the location and host rock of the samples.

Crushing, homogenization and splitting of the samples were carried out at the Department of Earth Sciences, Uppsala University. The samples were milled with a TM Engineering mildsteel ring-and-puck pulverizer and analysed chemically at Acme Labs in Vancouver, Canada using inductively coupled plasma (ICP)

https://doi.org/10.1017/S0016756813000551 Published online by Cambridge University Press

Table 1. Sample locations and descriptions (Swedish National Coordinate Net 2.5 Gon V, RT90)

Sample	Host rock	Easting	Northing
20	Meta-volcanite	1612115	6679030
26	Meta-volcanite	1612510	6679480
27	Meta-volcanite	1613015	6679600
81	Meta-volcanite	1615140	6680880
87	Marble and metavolcanite	1613535	6677515
111B	Metavolcanite	1610815	6679990
122	Metagranitoid	1615770	6680095
123	Metagranitoid	1615365	6680735
76	Metavolcanite	1616850	6680330
276–138	Metavolcanite		
276–146	Metavolcanite		
276–164	Metavolcanite		
276–28	Metavolcanite		
286–5	Metavolcanite		
494–1177	Metavolcanite		
494–213	Metavolcanite		
494–629	Metavolcanite		
494–675	Metavolcanite		

emission spectrometry for major elements and inductively coupled plasma – mass spectrometry (ICP-MS) for trace elements (Table 2).

Twelve of the 18 samples, including sample 076, were selected for Sr and Nd isotopic analyses. The samples were milled with an agate pulverizer at the Department of Earth Sciences, Uppsala University. The analyses were carried out at the Laboratory for Isotope Geology, Swedish Museum of Natural History. About 100–200 mg of rock powder from each sample was dissolved in Teflon capsules at 205 °C for a few days in a 10:1 mixture of concentrated HF and HNO_3. Before digestion a mixed ^{147}Sm–^{150}Nd spike was added. After evaporation and redissolution in 6 M HCl, the solutions were passed through TRU-spec columns for separation of Sr and Rare Earth Elements (REE) as a group, and Sr further purified in Sr-spec columns. From the REE solutions, Sm and Nd were separated using Ln-spec columns (Pin & Zalduegui, 1997).

The samples were loaded on double Re filaments and analysed with a Thermo Triton thermal ionization mass spectrometer. The concentrations of Sm and Nd were determined by isotope dilution using the combined ^{147}Sm–^{150}Nd spike, whereas the Rb and Sr contents reported by Acme Labs were used for calculation of initial Sr isotope composition. Corrections for background, spike addition, interference and fractionation were carried out and are reported in the footnotes to Table 3. The results are shown in Table 3, together with results on the NBS SRM987 Sr standard and the La Jolla Nd standard.

4 Results

4.a Field observations and petrography

The mafic dykes are very fine grained and have a light greenish-grey to greyish-green tint on weathered surfaces, whereas fresh surfaces are darker grey. Their widths vary from a few decimetres to more than a metre, with apophyses a couple of centimetres wide occurring in places. The strike and dip of the dykes sampled in drill cores could not be derived; field sampling was however accompanied by measurements of strike and dip, and the orientation of the dykes varies a lot around a fold axis dipping *c.* 65° towards the NW (P. Dahlin, unpubl. data, 2013). The contacts between dykes and host rocks are always sharp and chilled margins have been recorded at scattered locations (Fig. 3a). Dykes within supracrustal rocks are generally discordant, albeit with a low angle to the bedding, but high angles may occasionally be seen (Fig. 3b). The dykes generally display varying amounts of deformation such as boudinage (Fig. 3c), but in outcrop scale folds are rarely seen. Dykes within metagranitoid host rocks always have straight contacts and are not boudinaged. One recorded dyke contains fragments of the metavolcanic host rock (Fig. 3d). Decimetre-wide bleached zones in the wall rock have been recorded around some of the dykes.

Symmetric <10 mm Ø vugs are common on weathered surfaces and must have formed after the deformation (otherwise they would have been elliptical in shape). The size of the vugs decreases from the centres of the dykes and outwards (Fig. 3a) and it is not uncommon that plagioclase phenocrysts vary in size in a similar way; these vugs are probably holes after weathered plagioclase crystals. The dominating minerals in the rocks are epidote and chlorite with subordinate amphibole, sericite, calcite, quartz and titanite. Sample 087, which is hosted by marble and metavolcanic rocks, is the only one dominated by amphibole. Plagioclase phenocrysts occur as completely saussuritized aggregates consisting of epidote and sericite. Sparse euhedral pyrite grains, <1 mm in size, are the main opaque phase.

4.b Geochemistry

The SiO_2 concentrations show a narrow range between 46 and 51 wt % with two exceptions: sample 087 with SiO_2 of 43 wt % and sample 076 with 54 wt % SiO_2 (Table 2). Sample 087 has the highest concentration of Ca of all samples and very low contents of Na, K, Rb and Ba. It comes from a dyke partly hosted by marble, with which it may have undergone metasomatic exchange. Sample 076 comes from a rock interpreted to be of volcanic origin by Stålhös (1991), and appears to deviate geochemically from the dykes.

A significant metasomatic alteration of the dykes is indicated when plotted in Hughes' igneous spectrum (Fig. 4a; Hughes, 1972), where all samples except 076 plot outside the defined field of magmatic compositions. Samples that cluster close to the igneous spectrum are grouped as least altered and the rest as altered. This division is used in subsequent diagrams. The total alkali content is fairly constant for most samples, but an increasing dominance of K_2O over Na_2O is seen as a shift towards the right in the diagram for the altered samples (Fig. 4a). In a diagram of K_2O versus Na_2O the

https://doi.org/10.1017/S0016756813000551 Published online by Cambridge University Press

Table 2. Geochemical analyses of the Dannemora samples

Sample no.	087	286–5	123	276–164	276–138	494–213	111 B	020	494–629	122	276–146	494–1177	027	081	276–28	026	494–675	076
SiO_2 (wt %)	41.76	44.23	45.15	44.23	44.61	45.21	47.17	48.32	46.88	46.49	48.87	45.41	45.97	46.59	44.50	45.71	48.26	53.50
TiO_2	1.03	1.18	1.22	0.94	0.91	1.06	0.83	0.82	1.00	0.81	1.01	1.32	0.82	0.95	0.87	1.01	0.90	0.76
Al_2O_3	14.37	15.66	16.37	12.97	17.26	14.64	16.29	14.67	12.56	14.95	16.41	15.28	17.89	15.88	14.20	15.00	16.78	15.99
Fe_2O_3-tot	13.32	13.07	13.28	12.20	12.07	13.27	11.86	11.76	9.97	10.53	12.05	11.94	11.50	11.77	10.77	10.93	10.43	9.19
MnO	1.04	0.20	0.37	0.25	0.26	0.21	0.20	0.15	0.19	0.21	0.23	0.41	0.16	0.19	0.25	0.13	0.20	0.14
MgO	9.71	7.96	6.39	10.49	5.29	8.38	6.39	8.38	10.6	6.27	4.67	8.14	6.12	8.96	7.04	6.91	5.33	4.76
CaO	14.84	12.49	10.01	10.41	9.72	9.72	9.02	7.88	9.21	9.85	8.45	10.56	11.49	8.40	10.08	9.47	9.88	9.95
Na_2O	0.14	0.64	0.62	0.53	0.74	0.84	1.51	1.13	0.91	1.24	0.90	1.92	1.32	2.13	1.42	1.37	1.49	3.35
K_2O	0.09	0.47	2.80	0.87	2.33	0.80	1.58	2.90	1.73	1.87	2.23	1.23	0.79	1.26	0.89	0.72	0.79	0.67
P_2O_5	0.34	0.17	0.22	0.14	0.19	0.35	0.20	0.16	0.17	0.21	0.19	0.23	0.18	0.14	0.26	0.30	0.21	0.09
Cr_2O_3	0.060	0.021	0.008	0.105	0.005	0.039	0.013	0.096	0.148	0.009	0.003	0.040	0.013	0.040	0.029	0.016	0.011	0.007
LOI	3.0	3.6	3.3	6.6	6.4	5.2	4.7	3.4	6.3	7.3	4.8	3.2	3.5	3.4	9.5	8.2	5.5	1.4
Sum	99.70	99.69	99.74	99.74	99.79	99.72	99.76	99.67	99.67	99.74	99.81	99.68	99.75	99.71	99.81	99.77	99.78	99.81
TOT/C	<0.02	0.2	0.2	0.7	0.6	0.4	0.3	0.3	0.6	1.1	0.2	0.2	0.2	0.2	1.4	1.2	0.5	0.2
TOT/S	<0.02	0.1	<0.02	0.1	0.2	0.0	0.1	0.2	0.0	<0.02	0.0	<0.02	0.0	<0.02	<0.02	0.4	<0.02	<0.02
Sc (ppm)	46	48	39	43	48	40	43	38	33	38	34	45	45	39	37	43	34	37
Ba	28	93	309	129	356	151	471	491	191	260	271	364	199	257	91	72	87	233
Be	<1	<1	2	<1	<1	<1	<1	<1	<1	<1	<1	<1	<1	<1	1	<1	<1	<1
Co	39.4	48.3	38.6	46.6	39.8	40.1	34.1	35.8	42.8	35.4	26.1	41.3	25.9	42.5	25.9	38.8	22.5	27.8
Cs	<0.1	0.1	2.1	0.2	0.4	0.2	2.2	1.3	0.2	1.5	1.6	0.6	0.1	0.3	0.4	0.5	0.3	0.4
Ga	13.6	16.1	18.2	13.1	17.3	16.3	14	18.7	13.5	15	17.2	14.8	17.4	14.5	13.9	16	15.5	15
Hf	2.3	1	1.5	1.2	1.4	1.3	1.9	2	1.9	1.8	1.8	1.7	0.9	1.4	1.6	2.2	1.6	1.2
Nb	7.4	1.9	3.3	2.5	2.2	2.4	4.3	6.5	7.4	5.2	3.9	4.6	1.8	3.4	3.3	6.8	3.6	2.4
Rb	0.8	13.5	171.3	24	80.7	18.3	80.1	98.6	53.7	85.1	152.3	48.9	23.5	44.3	32.3	27.2	33	16
Sn	2	<1	1	<1	<1	<1	<1	3	<1	<1	<1	1	3	1	<1	1	<1	<1
Sr	216.2	573.8	208.9	215.4	328.4	558.1	335.6	293.9	203.5	308.5	345.5	399.1	470.6	198.6	150.8	258.7	407.2	347.2
Ta	0.4	0.2	0.2	0.2	0.2	0.1	0.2	0.4	0.6	0.3	0.3	0.2	0.1	0.2	0.2	0.3	0.2	0.2
Th	0.9	0.6	0.8	0.6	1.8	1.3	1.4	2.1	2.7	1.9	2.5	0.4	0.6	0.8	1.1	1.0	1.2	2.3
U	0.4	0.5	0.3	0.3	0.7	0.7	0.8	0.8	1.0	0.7	1.0	0.3	0.4	0.3	0.4	0.5	0.7	0.8
V	269	425	329	264	288	273	243	259	231	254	232	303	299	262	222	282	225	209
W	1.2	0.7	1.2	<0.5	0.8	<0.5	0.7	<0.5	0.6	<0.5	0.6	0.6	<0.5	1.1	<0.5	0.5	0.5	<0.5
Zr	90.5	33.8	46.5	38.1	49.1	40.6	65.7	69.6	62.0	62.1	72.0	61.0	29.7	49.9	56.3	85.2	51.1	38.0
Y	19.0	8.0	13.2	12.7	10.2	14.3	15.1	16.2	14.1	15.0	11.9	15.9	8.7	12.9	15.2	19.4	11.4	12.2
La	16.2	7.1	9.3	5.2	10.2	8.8	10.6	12.4	11.5	11.5	15.6	7.7	6.3	7.3	9.5	14.8	9.6	7.2
Ce	36.9	14.1	20.7	12.6	23.3	20.9	22.4	27,0	25,0	25.4	34.1	18.3	14.6	16.8	23,0	33.8	21.4	17.6
Pr	4.95	2.08	2.82	1.72	2.98	3.02	3.15	3.39	3.20	3.37	4.11	2.58	2.02	2.27	3.09	4.59	2.93	2.40
Nd	21.4	8.6	11.5	8.7	12.8	15.1	13.9	14.4	12.9	14.7	18.1	12.1	9.4	9.8	14.6	19.9	12.3	10.3
Sm	4.46	2.07	2.77	2.19	2.49	3.29	3.03	3.14	2.85	3.10	3.21	2.98	2.17	2.33	3.09	4.17	2.68	2.53
Eu	1.68	0.85	1.04	0.80	0.92	1.00	1.05	1.08	0.88	0.91	1.04	1.12	0.86	0.85	0.98	1.42	1.01	0.79
Gd	4.02	1.94	2.66	2.34	2.23	3.11	2.98	3.14	2.80	2.99	2.71	3.09	2.01	2.35	3.01	4.02	2.50	2.36
Tb	0.64	0.28	0.43	0.42	0.36	0.50	0.48	0.51	0.47	0.50	0.42	0.54	0.30	0.39	0.51	0.61	0.39	0.38
Dy	3.18	1.46	2.44	2.55	2.01	2.65	2.62	2.89	2.53	2.68	2.45	3.00	1.51	2.25	3.17	3.35	2.06	2.14
Ho	0.66	0.28	0.50	0.49	0.36	0.54	0.52	0.61	0.51	0.54	0.45	0.60	0.32	0.47	0.59	0.68	0.41	0.44
Er	1.90	0.85	1.41	1.52	1.15	1.45	1.75	1.64	1.51	1.48	1.35	1.78	0.89	1.42	1.79	1.87	1.16	1.23
Tm	0.29	0.11	0.22	0.22	0.17	0.22	0.22	0.27	0.22	0.24	0.19	0.25	0.13	0.21	0.25	0.29	0.16	0.18
Yb	1.74	0.86	1.39	1.39	1.09	1.30	1.50	1.68	1.35	1.49	1.24	1.58	0.82	1.32	1.50	1.83	1.08	1.16
Lu	0.28	0.12	0.22	0.21	0.16	0.19	0.22	0.25	0.21	0.23	0.19	0.24	0.12	0.20	0.23	0.28	0.16	0.18
Mo	0.7	0.3	0.9	0.3	0.4	0.4	0.3	0.4	0.6	0.5	0.9	0.4	0.3	0.2	0.3	0.5	0.4	0.2
Cu	2.5	35.1	2.3	4.0	4.8	22.6	33.1	45.8	14.0	35.2	6.0	21.3	5.2	2.2	0.6	8.0	28.8	6.0
Pb	3.8	5.7	1.9	0.4	0.9	1.0	1.4	0.8	1.2	1.6	0.7	45.3	0.9	1.5	0.3	0.8	1.3	0.9
Zn	99	67	87	71	75	78	73	69	48	97	80	129	37	53	72	55	77	18
Ni	32.7	24.2	26.1	58.0	8.3	75.6	12.6	69.1	134.6	11.1	7.6	28.4	11.7	39.7	37.2	10.7	13.2	5.0
As	50.3	5.4	10.6	1.0	4.2	2.2	1.1	0.8	3.3	2.0	1.2	27.5	6.5	1.1	3.0	3.2	27.8	0.7
Sb	0.7	0.1	0.2	0.1	0.2	0.1	<0.1	0.1	0.2	<0.1	0.2	0.7	0.2	0.1	<0.1	<0.1	0.3	0.1
Bi	0.1	<0.1	<0.1	<0.1	0.1	<0.1	<0.1	<0.1	<0.1	<0.1	<0.1	0.2	<0.1	0.2	<0.1	0.1	<0.1	0.1
Ag	<0.1	<0.1	<0.1	<0.1	<0.1	<0.1	<0.1	<0.1	<0.1	<0.1	<0.1	0.1	<0.1	<0.1	<0.1	<0.1	<0.1	<0.1
Tl	<0.1	<0.1	0.3	<0.1	<0.1	<0.1	<0.1	0.2	<0.1	<0.1	0.5	<0.1	<0.1	<0.1	<0.1	<0.1	<0.1	<0.1
Au (ppb)	<0.5	<0.5	<0.5	<0.5	2.2	0.9	<0.5	<0.5	<0.5	<0.5	0.6	<0.5	<0.5	<0.5	<0.5	<0.5	1.1	<0.5
Tot-REE	98.3	40.7	57.4	40.4	60.2	62.1	64.4	72.4	65.9	69.1	85.2	55.9	41.5	48.0	65.3	91.6	57.8	48.9
Mg#	60	56	50	64	48	57	53	60	69	56	45	59	53	61	58	57	52	52
Eu/Eu*	1.25	1.34	1.21	1.11	1.23	0.98	1.10	1.08	0.98	0.94	1.11	1.16	1.30	1.14	1.01	1.09	1.23	1.02
(La/Yb)n	6.7	5.9	4.8	2.7	6.7	4.9	5.1	5.3	6.1	5.5	9.0	3.5	5.5	4.0	4.5	5.8	6.4	4.5
(La/Sm)n	2.3	2.2	2.2	1.5	2.6	1.7	2.3	2.5	2.6	2.4	3.1	1.7	1.9	2.0	2.0	2.3	2.3	1.8
(Gd/Yb)n	1.9	1.9	1.6	1.4	1.7	2.0	1.6	1.5	1.7	1.7	1.8	1.6	2.0	1.5	1.7	1.8	1.9	1.7

altered samples tend to plot outside fields for magmatic compositions (Fig. 4b).

The Mg number ($100 \times$molar $Mg/(Mg+Fe^{2+})$, assuming that $Fe^{2+} = 0.85 \times Fe_{tot}$) ranges from 71 to 47. The MgO content varies between 4.8 and 11.3 wt %. In Figure 5, MgO has been used as a differentiation index. Most of the major elements show no distinct trends with respect to decreasing MgO and no systematic difference between altered and least-altered samples (except for Na_2O and K_2O). For SiO_2, a slight increase

https://doi.org/10.1017/S0016756813000551 Published online by Cambridge University Press

Table 3. Sr and Nd isotope data for the Dannemora dykes plus basalt sample 076

No.	Sample no.	$^{87}Rb/^{86}Sr$[1]	$^{87}Sr/^{86}Sr \pm 2\sigma_m$[2] (measured)	$^{87}Sr/^{86}Sr$ (1870)	ε_{Sr}[3] (1870)	T_{UR}[3] (Ga)	Sm[4] (ppm)	Nd[4] (ppm)	$^{147}Sm/^{144}Nd$[4]	$^{143}Nd/^{144}Nd \pm 2\sigma_m$[5] (measured)	ε_{Nd}[6] (present)	ε_{Nd}[6] (1870)	T_{CHUR}[7] (Ga)	T_{DM}[8] (Ga)
1	087	0.0107	0.704064 ± 4	0.70378	21.4	0.43	4.71	22.05	0.1291	0.511829 ± 2	− 15.8	0.4	1.82	2.18
2	276–164	0.3225	0.713354 ± 4	0.70467	34.2	2.55	2.32	8.48	0.1654	0.512335 ± 4	− 5.9	1.6	1.48	2.24
3	276–28	0.6205	0.719994 ± 6	0.70330	14.6	2.00	3.30	14.29	0.1397	0.511971 ± 3	− 13.0	0.6	1.78	2.21
4	494–213	0.0949	0.705779 ± 6	0.70323	13.6	7.05	3.66	15.01	0.1476	0.512069 ± 3	− 11.1	0.7	1.77	2.25
5	494–1177	0.3546	0.711268 ± 5	0.70173	− 7.8	1.73	3.21	12.96	0.1497	0.512123 ± 2	− 10.0	1.2	1.67	2.19
6	026	0.3043	0.710795 ± 5	0.70261	4.7	1.97	4.28	19.80	0.1307	0.511865 ± 2	− 15.1	0.7	1.78	2.16
7	027	0.1445	0.707614 ± 5	0.70373	20.7	3.46	2.17	9.31	0.1408	0.512005 ± 4	− 12.3	1.1	1.72	2.17
8	122	0.7994	0.724747 ± 5	0.70323	13.7	1.96	3.21	14.43	0.1344	0.511914 ± 3	− 14.1	0.8	1.77	2.17
9	081	0.6464	0.723516 ± 5	0.70612	54.8	2.34	2.31	9.83	0.1419	0.511994 ± 3	− 12.6	0.6	1.79	2.23
10	494–675	0.2345	0.710818 ± 7	0.70451	31.8	2.87	2.95	13.26	0.1345	0.511910 ± 2	− 14.2	0.7	1.78	2.18
11	020	0.9728	0.730795 ± 5	0.70462	33.3	2.05	3.06	13.54	0.1367	0.511940 ± 3	− 13.6	0.8	1.77	2.18
12	076	0.1333	0.706957 ± 5	0.70337	15.6	3.34	2.56	10.67	0.1448	0.512036 ± 3	− 11.7	0.7	1.77	2.23

[1] $^{87}Rb/^{86}Sr$ ratio based on chemical analyses of Rb and Sr by Acme Analytical Laboratories, Vancouver, Canada (Table 2).
[2] $^{87}Sr/^{86}Sr$ ratios measured on a Thermo Triton thermal ionization mass spectrometer in static mode, corrected for Rb interference and normalized to $^{86}Sr/^{88}Sr = 0.1194$. Two runs of the NBS SRM 987 Sr-standard during the measurement periods gave $^{87}Sr/^{86}Sr$ ratios of 0.710211 ± 7 and 0.710231 ± 5 ($2\sigma_m$). Error given as 2 standard deviations of the mean from the mass spectrometer run in the last digits.
[3] ε_{Sr} values (at 1870 Ma) and T_{UR} Sr model ages according to McCulloch & Chappell (1982): present-day $^{87}Rb/^{86}Sr$ mantle ratio = 0.0827, present-day $^{87}Sr/^{86}Sr$ mantle ratio = 0.7045.
[4] Sm and Nd contents and $^{147}Sm/^{144}Nd$ ratio from isotope dilution analysis with combined $^{147}Sm/^{150}Nd$ tracer. Estimated analytical uncertainty of $^{147}Sm/^{144}Nd$ ratio is ± 0.5%.
[5] Sm and Nd measured with a Thermo Triton thermal ionization mass spectrometer in static mode. $^{143}Nd/^{144}Nd$ ratios calculated from ID run, corrected for Sm interference and normalized to $^{146}Nd/^{144}Nd = 0.7219$. Twelve runs of the La Jolla Nd-standard during a period of 8 months around the measurement period gave a $^{143}Nd/^{144}Nd$ ratio of 0.511863 ± 9 (2σ, external precision). Error given as 2 standard deviations of the mean from the mass spectrometer run in the last digits.
[6] Present-day and initial ε_{Nd} values (at 1870 Ma) calculated using a present-day chondritic $^{147}Sm/^{144}Nd$ ratio of 0.1966, and a present-day chondritic $^{143}Nd/^{144}Nd$ ratio of 0.512638 (cf. Dickin 1995). Overall uncertainty in initial ε_{Nd} value estimated to ± 0.5 ε units.
[7] Model age calculated relative to the chondritic uniform reservoir (CHUR) of Jacobsen & Wasserburg (1984) (recalculated as in Dickin, 1995).
[8] Model age calculated relative to the depleted mantle curve (DM) of De Paolo (1981).

from *c.* 47 to *c.* 50 wt % (disregarding the outliers of samples 076 and 087) may be discerned. The content of Al_2O_3 increases from *c.* 14 to *c.* 18 wt %, CaO scatter in the interval 8–13 wt %, and FeO-tot cluster around 11 wt %. Among the trace elements, Ga shows an increase similar to that of Al_2O_3, from *c.* 14 to 18 ppm. Cobalt decreases from *c.* 45 to 25 ppm with decreasing MgO, Cr shows a very marked decrease from >1000 ppm to *c.* 20 ppm, and Ni a strong decrease from 150 to *c.* 10 ppm. Vanadium and Sc display flat trends at *c.* 200–300 ppm and 35–50 ppm, respectively. Many other trace elements, e.g. Rb, Ba and Sr, but also more immobile incompatible trace elements scatter when plotted against MgO (Fig. 5) but show good linear trends in Figure 6 (e.g. Zr, Y, Ce and other REE).

In Figure 6, major and selected trace elements have been plotted against Nb. Elements such as SiO_2, FeO, CaO, TiO_2 and Al_2O_3 show semi-horizontal trends, whereas MgO, K_2O and Na_2O scatter. The trace elements Ce, Zr and Nd plot with positive slope relative to Nb and Sr with a negative slope, whereas the elements Ba, Rb and Th scatter.

The total REE contents are between 40 and 100 ppm. Normalized to chondrite, the $(La/Yb)_n$ range between 2.7 and 9.0, $(La/Sm)_n$ between 1.5 and 3.1 and $(Gd/Yb)_n$ between 1.4 and 2.0 (Table 2; Fig. 7a). The strongest REE enrichment is seen for the carbonate-hosted dyke 087 and sample 026. Sample 276-146 shows higher enrichment mainly in the light REE (LREE). Samples 027 and 286-5 show less enrichment in heavy REE (HREE) than the others. The Eu-anomaly ranges between 0.90 and 1.28, mostly positive, suggesting some accumulation of plagioclase during crystallization or contamination by the lower crust. The trace element variation diagram shows enrichment in large-ion lithophile elements (LILE) such as K, Rb and Ba as well as Th, and troughs for Ta–Nb and Zr–Hf (Fig. 7b), as is typical for subduction-related rocks (e.g. Pearce & Peate, 1995; Davidson, 1996). Sample 087 has a divergent pattern with K and Rb just above 1 and Ba *c.* 5.

4.c Isotopes

The Sr and Nd isotope data of the 12 analysed samples are displayed in Table 3. The Rb contents show a wide range between 0.8 ppm (for the marble-hosted dyke 087) and *c.* 100 ppm, whereas the Sr contents range between 155 and 575 ppm, yielding $^{87}Rb/^{86}Sr$ ratios of 0.0107–0.9728. The measured ratios of $^{87}Sr/^{86}Sr$ range from 0.704064 to 0.730795, whereas the initial $^{87}Sr/^{86}Sr$ ratios calculated using ICP-MS data at an assumed age of 1870 Ma scatter between 0.70173 and 0.70612, corresponding to an initial ε_{Sr} of –8 to +55. The Sm concentrations vary between 2.2 and 4.7 ppm and Nd between 8.5 and 22.1 ppm, resulting in $^{147}Sm/^{144}Nd$ ratios of 0.1291–0.1654. The present-day measured ratios of $^{143}Nd/^{144}Nd$ fall between 0.511829 and 0.512335, and the initial ε_{Nd} values calculated at 1870 Ma fall between +0.4 and +1.6 (Fig. 8). A Sm–Nd isochron calculation through all 12 points yields an imprecise age of 2064 ± 110 Ma (2σ, MSWD 2). This age is about 200 Ma older than the geological age of the dykes.

https://doi.org/10.1017/S0016756813000551 Published online by Cambridge University Press

Figure 3. (Colour online) (a) Dyke with vugs (encircled) and chilled margins at both contacts to the metavolcanic rock. The width of the chilled margins is highlighted with black lines and one arrow. Pen for scale is 15 cm long. Location is south of Bennbo (cf. Fig. 2). (b) Discordant relationship between dyke and laminated ash-siltstone (indicated by broken lines). Notice the almost perpendicular angle between the two silicate rock types, whereas in the marble the dyke has a lower angle to the bedding. From a drift in the ceiling at 175 m depth in the Dannemora mine. (c) Dyke divided into two boudins and an apophysis (highlighted by broken line). Location is north of Bennbo (cf. Fig. 2). (d) Dyke with a large completely enclosed metavolcanic fragment from sample site 026 (cf. Table 1).

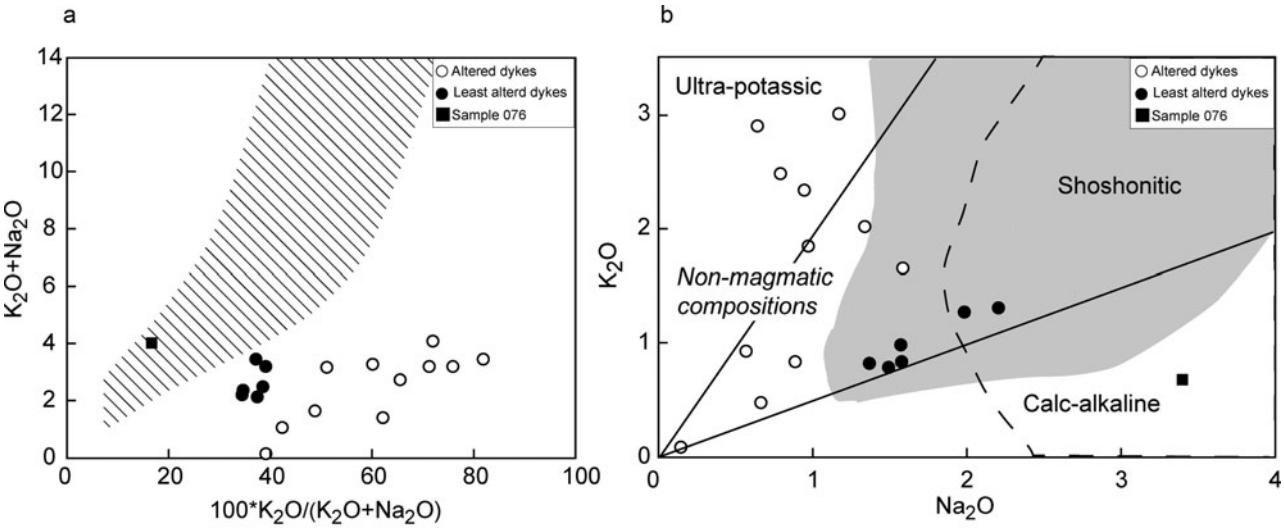

Figure 4. (a) Igneous spectrum diagram after Hughes (1972). Striped field defines magmatic composition of non-altered rocks. The least-altered rocks cluster close to the igneous spectrum field, whereas the more-altered rocks scatter along the *x*-axis. (b) Diagram showing K_2O versus Na_2O. The grey field represents *c.* 1.8 Ga mafic rocks (excluding ultrabasites) from the Transscandinavian Igneous Belt (TIB) and post-collisional shoshonitic rocks from further east in the Fennoscandian Shield (see Andersson *et al*. 2006*b*; Rutanen *et al*. 2011) as examples of magmatic alkali-rich compositions. Other shoshonitic and ultrapotassic igneous rocks plot at signifcantly higher Na_2O and K_2O compositions (e.g. Turner *et al.* 1996; Miller *et al.* 1999; Zhang *et al.* 2008; Zhao *et al.* 2009). The dashed line encloses other rocks with magmatic composition (Pe-Piper, 1983; Meen, 1987; Leslie *et al.* 2009; Ishizuka *et al.* 2010; Yang *et al.* 2012). Most of the altered samples also plot outside magmatic compositions.

https://doi.org/10.1017/S0016756813000551 Published online by Cambridge University Press

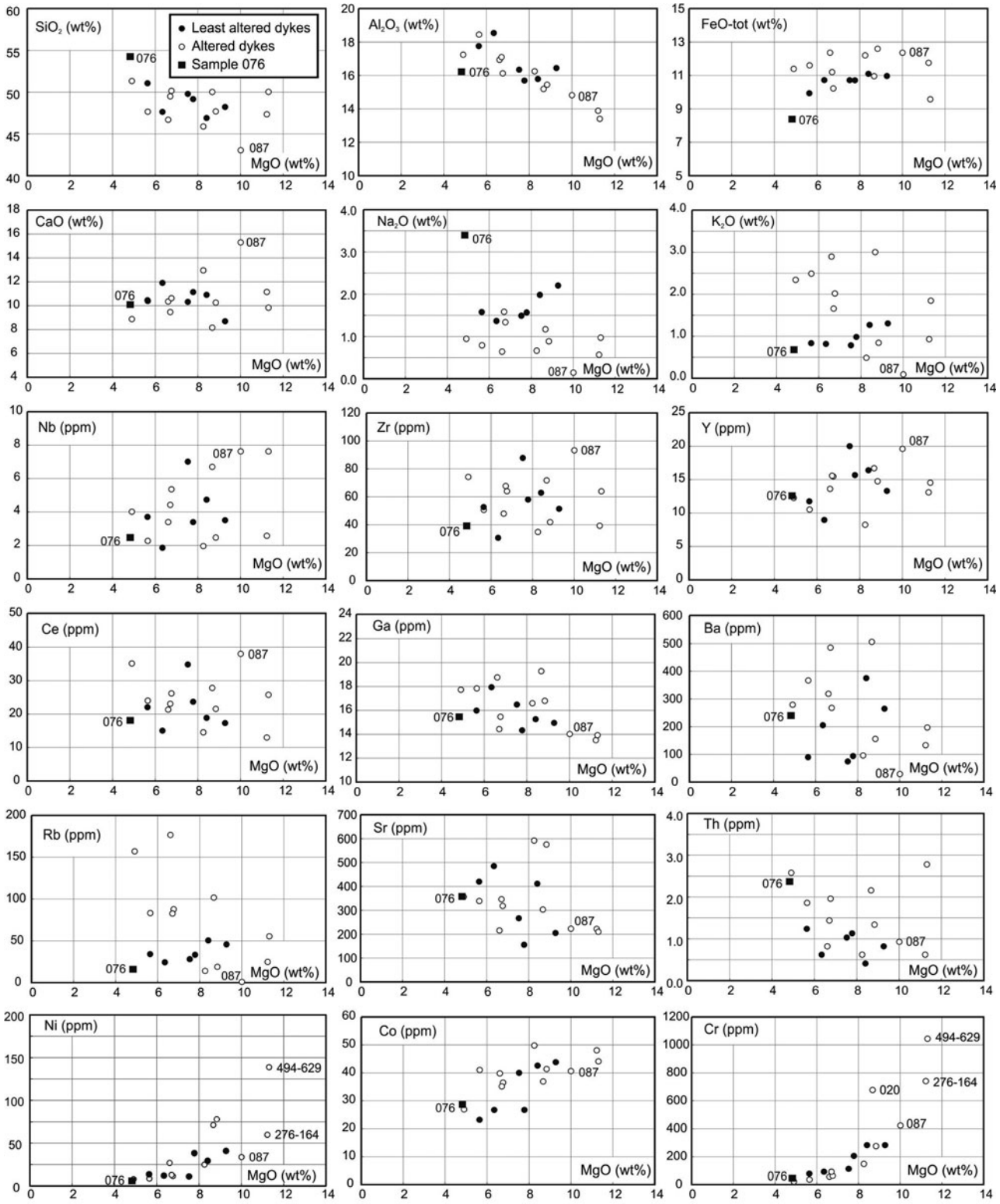

Figure 5. Selected major and trace elements plotted against MgO. Differentiation (fractionation) goes from right to left as MgO decreases during differentiation. Samples 076 (basaltic amphibolite: filled square) and 087 (altered mafic dyke partly hosted by marble) have been specially marked.

5 Discussion

5.a Age of the Dannemora dykes

The absolute age of the Dannemora dykes has not been determined. However, as the dykes are intruding both the supracrustal rocks and the surrounding granitoids, have been folded at least once and are metamorphosed in greenschist facies, they are inferred to be coeval with the second generation of dykes recognized by Stålhös (1991) and similar in age to the Herräng dykes and the mafic dykes in Forsmark, dated to between 1870 and 1860 Ma (Hermansson *et al.* 2008). The overall

https://doi.org/10.1017/S0016756813000551 Published online by Cambridge University Press

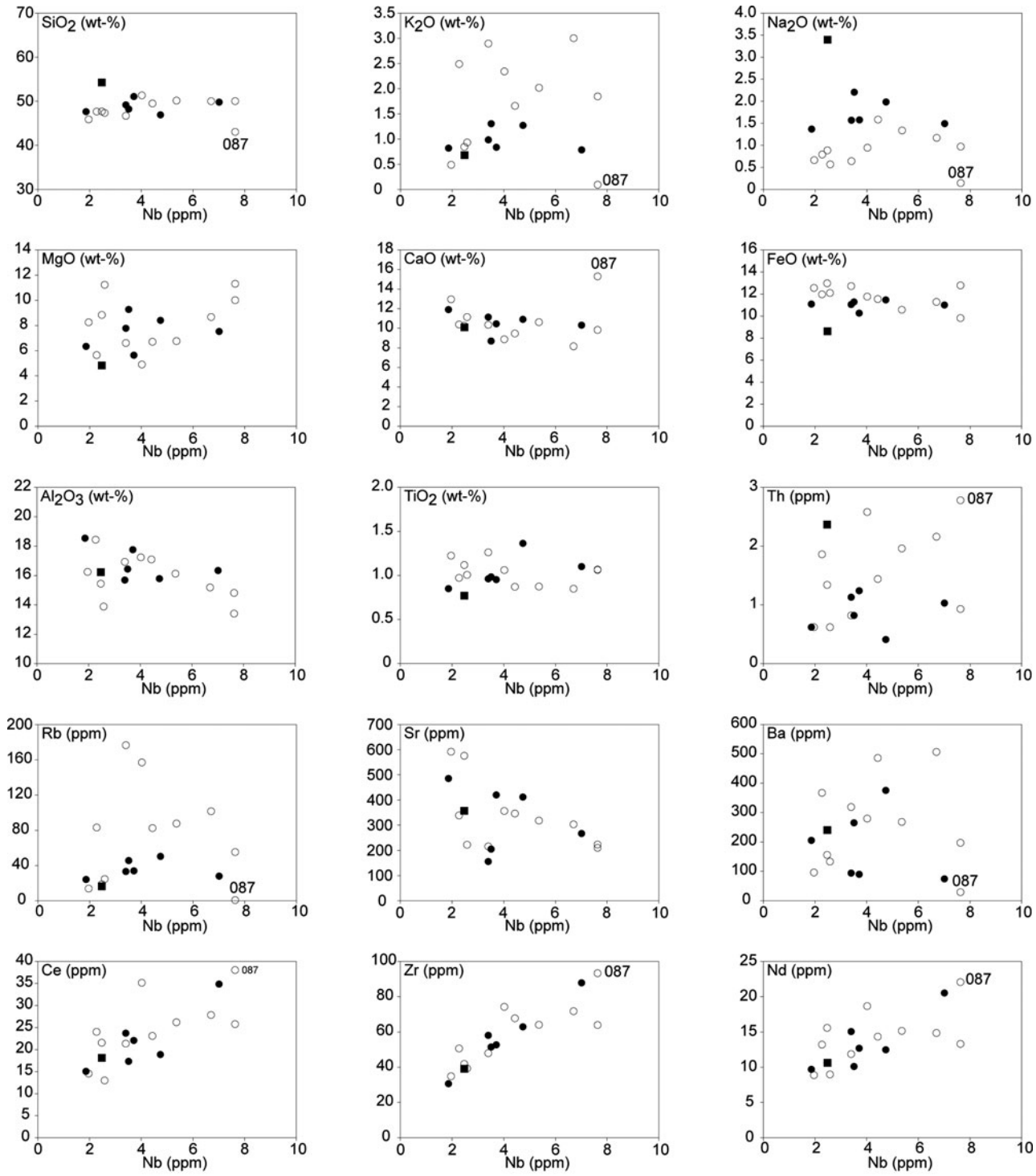

Figure 6. Selected major and trace elements plotted against the incompatible and immobile trace element Nb. Sample 076 is indicated by a filled square. Near linear trends in these diagrams probably reflect mixing with subordinate differentiation; scatter reflects disturbances of more mobile elements, or combined fractionation and mixing.

geochemical similarity suggests that all the sampled dykes in the Dannemora area belong to the same dyke swarm, and formed during a short period of time by the same magmatic processes.

The Sm–Nd isochron age of 2.06 ± 0.11 Ga and the T_{DM} model ages of 2.16–2.25 Ga for the individual samples do not reflect the age of intrusion for these dykes; instead, they may reflect the age of formation of the enriched source components or mixing between these components.

5.b Alteration and crustal contamination

The mobility of some major and trace elements during alteration, metamorphism and weathering is well documented (e.g. Nesbitt & Young, 1984, 1989; Sturchio

https://doi.org/10.1017/S0016756813000551 Published online by Cambridge University Press

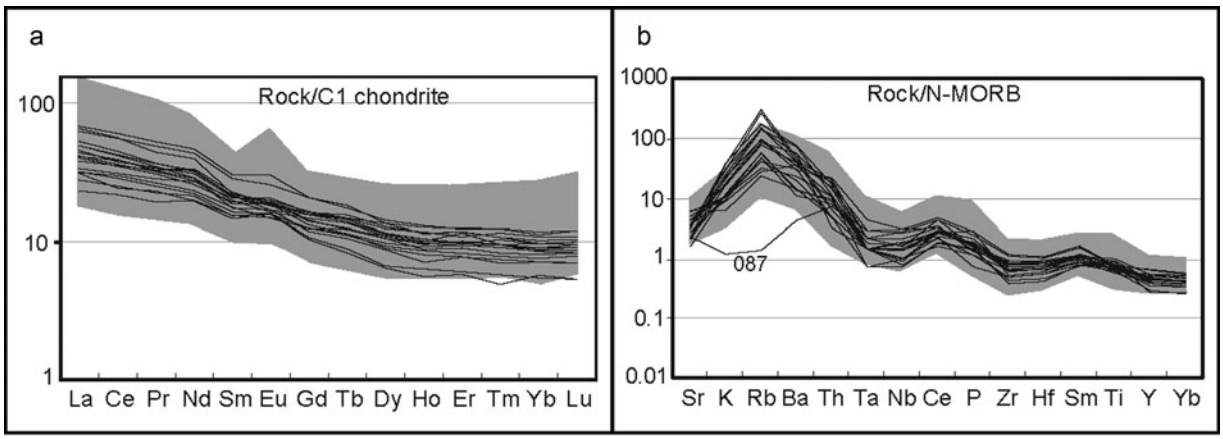

Figure 7. Trace and rare earth element variation diagrams. (a) REE normalized to C1/Chondrite. LREEs are mildly enriched compared to HREEs, with Eu anomalies between 0.90 and 1.28. Normalizing values from Sun & McDonough (1989). (b) Trace element variation diagram (spider-diagram) normalized to N-MORB, showing enriched values for the LILE and troughs for Ta–Nb and Zr–Hf. Normalizing values from Sun & McDonough (1989). The shaded areas show the compositions of the Avesta–Östhammar gabbros and diorites (Johansson & Hålenius, 2013).

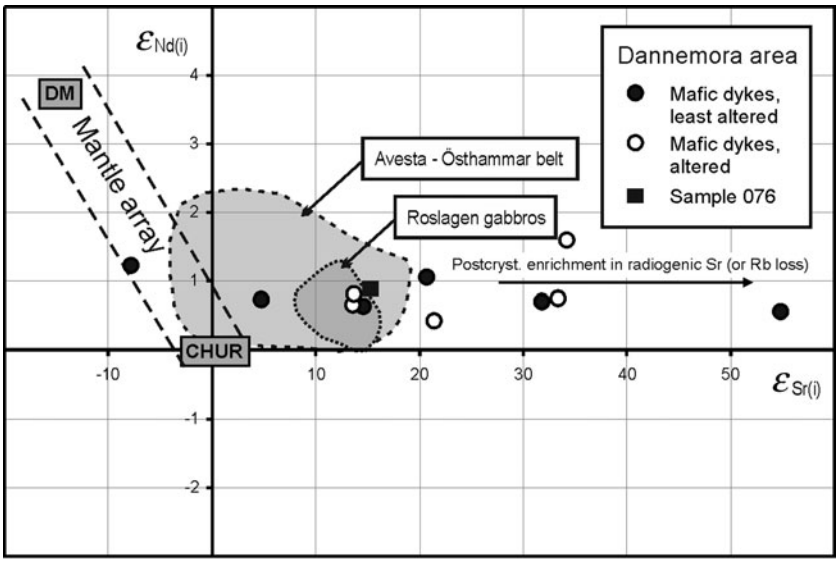

Figure 8. Initial ε_{Nd} versus initial ε_{Sr} for the Dannemora mafic dykes (at 1.87 Ga) and sample 076 (at 1.90 Ga), compared to the *c.* 1.89 Ga southern Roslagen gabbros (Johansson *et al.* 2012) and the gabbros and diorites of the Avesta–Östhammar belt (Johansson & Hålenius, 2013). CHUR – chondritic uniform reservoir; DM – depleted mantle. While having a small range of initial ε_{Nd} values, the Dannemora dykes show a much larger spread in initial ε_{Sr} towards the enriched side, possibly reflecting later disturbances in the Rb–Sr system.

et al. 1986). The strong enrichment in K_2O relative to Na_2O is not compatible with magmatic compositions of mafic rocks, as magmatic enrichment in K_2O is normally accompanied by enrichment in Na_2O (Fig. 4); instead, it suggests that the dykes have been subjected to post-magmatic alkali metasomatism with a resultant enrichment in K_2O and depletion in Na_2O. Breakdown of the magmatic plagioclase and depletion of the released Na during metamorphism, paired with an influx of external K (from the country rocks) accommodated in very fine-grained sericite, appears a possible explanation.

The metasomatism has also clearly affected Rb (cf. Fig. 5). Although not systematically depleted or enriched, metasomatism may also have affected other potentially mobile elements, e.g. Ba, Sr and Th. Petrogenetic interpretations of diagrams including these elements therefore have to be made with caution. The lack of systematic differences between altered and less-altered samples in the concentration of most elements (except the alkalis) however suggests that the original magmatic compositions have been largely retained during alteration. We therefore do not believe there was any systematic change in the concentration of MgO or of most other major or trace elements due to alteration. The interpretation of the geochemistry is, however, mainly based on immobile elements and/or the composition of the least-altered samples. High-field-strength elements (HFSE) such as Zr, Ti and Nb are usually immobile. Good linear trends for pairs of

https://doi.org/10.1017/S0016756813000551 Published online by Cambridge University Press

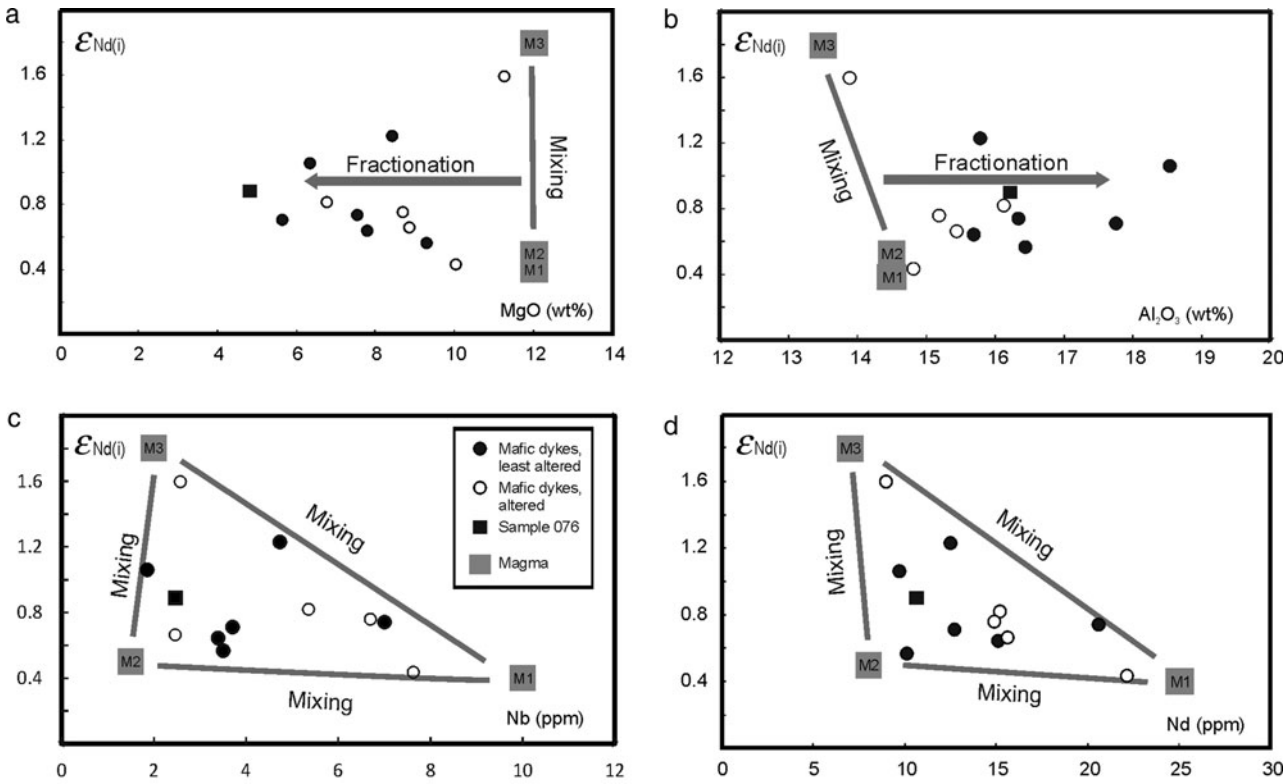

Figure 9. (a) Initial ε_{Nd} versus MgO concentration for the Dannemora dykes and basaltic amphibolite sample 076. (b) Initial ε_{Nd} versus Al_2O_3. (c) Initial ε_{Nd} versus Nb. (d) Initial ε_{Nd} versus Nd. The inferred mixing components (M1, M2, M3) and their fractionation and mixing trends are indicated. All three components have similar basaltic major element compositions, with *c.* 47–50 wt % SiO_2, 13.5–14.5 wt % Al_2O_3 and *c.* 12 wt % MgO, but differ in their incompatible trace element contents (exemplified by Nb and Nd) and their initial ε_{Nd} value. While the MgO and Al_2O_3 concentrations of the mixtures are strongly affected by fractionation (filled arrows), the incompatible trace elements are only slightly affected by fractionation but mostly by mixing (solid lines). The ε_{Nd} values are only affected by mixing and not at all by fractionation.

supposedly immobile elements suggest that they were indeed immobile in this case (Fig. 6; e.g. MacLean & Barrett, 1993).

The composition of sample 087 most likely reflects reactions with the surrounding marble, rather than an original primitive character with SiO_2 of *c.* 43 wt %. However, this sample generally does not plot as an outlier in immobile trace element plots. On the other hand sample 076 plots as an outlier in many diagrams and may therefore represent an older volcanic basalt flow unrelated to the dykes, as suggested by Stålhös (1991). However, no contacts have been recorded and the location of the outcrop within a regional-scale ductile deformation zone hinders further interpretation.

The geochemical data (e.g. displayed in Fig. 5) are not generally compatible with a model of bulk contamination by continental crust, which for example has higher HFSE at higher SiO_2. Moreover, the overall basaltic compositions suggest that the magmas were not contaminated by felsic crustal rocks, thereby indicating a short residence time for the magmas in the middle and upper crust before ascent and intrusion.

5.c Magmatic composition and evolution

Since MgO is strongly compatible and decreases with fractionation it is commonly used as a differentiation index for basaltic rocks. Niobium, on the other hand, is incompatible and usually immobile (e.g. MacLean & Barrett 1993; Hastie *et al.* 2007), and should therefore show an increase with increasing degree of fractionation. Diagrams with incompatible–incompatible elements, such as Zr versus Nb, display linear trends with positive slopes (Fig. 6). Such trends are also seen for diagrams with two compatible elements, e.g. MgO versus Co or Cr (Fig. 5). In contrast, diagrams showing incompatible–compatible elements for the same magmatic system, e.g. Nb versus MgO, should show negative slopes but tend to scatter in the present case (Fig. 5).

The strong decrease of the highly compatible elements MgO (from 12 to 5 wt %) and Cr (from >1000 to <50 ppm) with fractionation in the Dannemora dykes suggests crystallization of mafic minerals (olivine, chromite, pyroxene); consequently, the samples represent variable stages of fractionation of basaltic magma. However, the fractionation-controlled increase in incompatible elements in these basaltic melts was probably limited as long as most of the magma reservoir remained liquid. The linear trends seen in bivariate plots of Ce, Zr, Y and Yb versus Nb (Fig. 6) are not interpreted as differentiation trends, because such a process would result in a negative correlation between Nb and MgO. These trends are instead interpreted as the effect of mixing between at least two components with

https://doi.org/10.1017/S0016756813000551 Published online by Cambridge University Press

similar primitive major element compositions: one is less enriched in incompatible trace elements (e.g. 2 ppm Nb or less) and the other more enriched (e.g. 8 ppm Nb or more).The different dykes represent variable mixtures of the magma components that have differentiated to various stages.

The fractionation is best seen in plots combining two compatible 'mafic elements' such as MgO–Cr or MgO–Ni (Fig. 5) where they have a positive correlation, but also in some plots combining one compatible and one incompatible element such as MgO–Ga and MgO–Al_2O_3 (Fig. 5) provided that the different mixing components had similar concentrations of the elements involved. The mixing is best seen in plots of two immobile and incompatible elements such as Nb–Ce, Nb–Hf or Nb–Zr (Fig. 6), where the magma components had different starting compositions and the elements involved were little affected by fractionation. Combining MgO versus Nb or MgO versus Ce (Fig. 5), the analyses scatter as both processes are combined in a complex way in such plots with the variation of one element controlled by fractionation and the other by mixing.

The combined evidence from Figures 5 and 6 would suggest that, unlike MgO, Al_2O_3, Ga, Co, Ni and Cr, the distribution of most of the incompatible trace elements is not controlled primarily by fractionation, but by mixing between two or more components. Both Nd and Sm (not shown) show near-linear trends when plotted against Nb, indicating that these elements were immobile and that the Sm–Nd isotope system is intact. Unlike the chemical composition of magmas, the isotopic composition of Nd is not affected by fractionation, but only by mixing of different magmas and assimilation of wall rocks. In Figure 9 the initial ε_{Nd} values have been plotted against MgO, Al_2O_3, Nb and Nd. A triangular distribution of sample points suggests mixing between at least three components, M1, M2 and M3, which all have high MgO concentrations of *c.* 12 wt %. These components represents end-member magma compositions with distinct mantle sources. Note that there may be more than three mantle-derived components involved; these cannot be resolved, however. The position of each sample point within these diagrams represents a magma with a unique combination of mixing between these components and degree of fractionation. Data points shifted towards lower MgO and higher Al_2O_3 (Fig. 9a and b, respectively) represent magma batches of variably mixed and more evolved composition. In the other diagrams (Fig. 9c, d) the distribution of data points is mainly controlled by mixing between the three components, with only limited fractionation. Plotting of many such diagrams with elements in different combinations has made it possible to deduce the approximate end-member compositions of the three components.

These compositions are summarized in Table 4 (mixing components M1–M3). The major element composition of all three magmas is basaltic, although some differences can be discerned. M1 may be slightly higher in SiO_2 (*c.* 50 wt % versus 46–47 wt % in M2 and M3) and lower in CaO (8 versus 12 wt %). Above all, M1 is enriched in P and in many incompatible trace elements including Hf, Nb, Ta, Zr, Y and REE. Magma M2, on the other hand, is higher in K_2O, Na_2O, Rb, Ba and Cs. Magma M3 shows strong enrichment only in Sr. It also has a higher (more primitive) initial ε_{Nd} value of *c.* +1.8, whereas the two other magmas have isotopically more evolved Nd with ε_{Nd} values around +0.5 (Table 4). Even though the difference in initial ε_{Nd} is small, it is larger than the estimated analytical uncertainty of ± 0.5 ε units and is correlated with other geochemical characteristics, suggesting that it is real.

Table 4. Approximate composition of the proposed start magmas (mixing components M1–M3) and the inferred end magma (most-evolved magma)

	Mixing components			Most-evolved magma
	M1	M2	M3	
SiO_2 (wt %)	50	46	47	51
FeO-tot	13	10	12	11
Al_2O_3	14.5	14.5	13.5	18
MgO	12	12	12	5
CaO	8	12	12	10
Na_2O	1.0	2.5	1.0	1.0
K_2O	0.5	2.0	0.5	2.5
TiO_2	1.50	0.75	1.00	1.0
P_2O_5	0.41	0.14	0.14	0.2
MnO	0.3	0.1	0.2	0.2
Sum	**101.2**	**100.0**	**99.3**	**99.9**
Ba (ppm)	100	700	50	
P	1800	600	600	900
Cr	>1000	>1000	>1000	50
Co	50	50	50	25
Cs	0.2	0.5	0.2	
Ga	14	14	14	18
Hf	2.6	0.7	1.1	
Nb	10	1.5	2.0	
Rb	10	100	10	
Sr	100	100	600	400
Ta	0.55	0.10	0.15	
Th	1.5	0.5	0.3	
U	0.9	0.2	0.2	
Zr	100	25	35	
Y	23	7	12	12
Ni	150	150	75	10
La (ppm)	22	5	4	
Ce	45	12	10	
Pr	6	1.8	1.5	
Nd	25	8	7	
Sm	5.0	1.9	2.0	
Eu	1.8	0.7	0.7	
Gd	5.0	1.9	2.1	
Tb	0.80	0.25	0.35	
Dy	4.0	1.3	2.3	
Ho	0.83	0.25	0.47	
Er	2.40	0.65	1.35	
Tm	0.35	0.09	0.20	
Yb	2.10	0.50	1.30	
Lu	0.33	0.07	0.20	
$K_2O + Na_2O$	1.5	4.5	1.5	3.5
$100*K_2O/(K_2O+Na_2O)$	33	44	33	71
Mg number	66	72	68	49
$\varepsilon_{Nd}(i)$	0.4	0.5	1.8	0.9
$f_{(Sm/Nd)}$	−0.37	−0.25	−0.10	
$(La/Yb)_N$	7.5	7.2	2.2	
$(La/Sm)_N$	2.84	1.70	1.29	
$(Gd/Yb)_N$	1.97	3.14	1.34	
$(Eu/Eu*)_N$	1.09	1.11	1.04	

https://doi.org/10.1017/S0016756813000551 Published online by Cambridge University Press

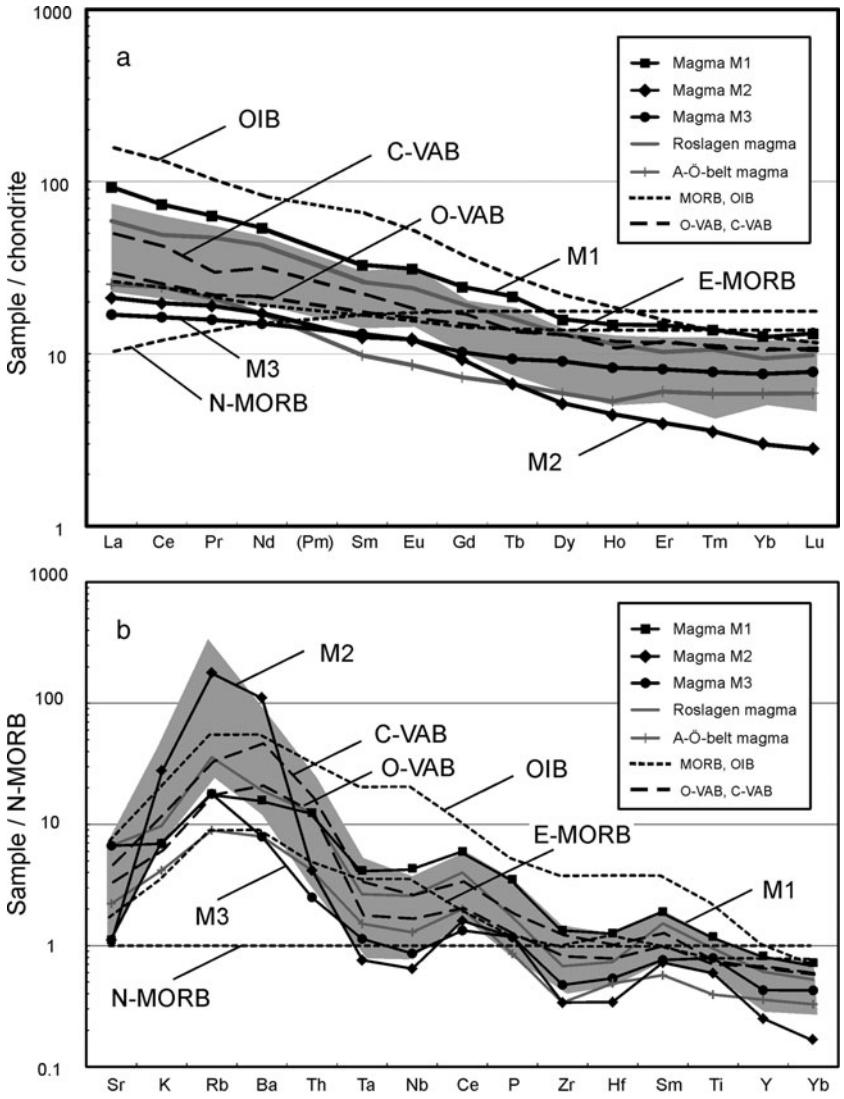

Figure 10. (a) REE and (b) trace element variation diagrams, showing the inferred compositions of the three magma components M1–M3 (Table 4). For comparison, the inferred start magmas for the Roslagen gabbro cumulates (Johansson *et al*. 2012) and the Avesta–Östhammar belt gabbros and diorites (Johansson & Hålenius, 2013) are also shown, as well as average compositions for E- and N-MORB and OIB (oceanic island basalts; Sun & McDonough, 1989) and continental and oceanic volcanic arc basalts (C-VAB and O-VAB; Kelemen *et al*. 2005). The shaded bands show the composition of the Dannemora dyke samples (the lines in Fig. 7a, b).

In Figure 10, the inferred rare earth and trace element compositions of the three magma components from Table 4 have been plotted in relation to the composition of the dyke samples (grey fields), the inferred start magmas for the Roslagen gabbro cumulates (Johansson *et al.* 2012) and the Avesta–Östhammar belt gabbros and diorites (Johansson & Hålenius, 2013), and average compositions for N-MORB (normal mid-ocean ridge basalt), E- (enriched-) MORB, OIB (ocean island basalt; Sun & McDonough, 1989) and oceanic and continental VAB (volcanic arc basalt; Kelemen *et al.* 2005). All of the three end-member magmas have their own character. Magma M1 stands out as most enriched in REE and HFSE. Magma M2 is strongly enriched in LILE (K, Rb and Ba, except Sr), but substantially less enriched in REE (especially HREE) and HFSE. Magma M3 is enriched in Sr but not in other LILE and HFSE, and has a much flatter (less-evolved) REE profile than the other magma components. All the three Dannemora end-member magmas are broadly similar to the inferred start magmas for the Roslagen gabbro cumulates (most similar to M1) and the Avesta–Östhammar belt gabbros and diorites (most similar to M3), and to the trace and rare earth element patterns of volcanic arc basalts with negative troughs for Ta–Nb and Zr–Hf (Fig. 10).

Compared to N-MORB all three magma components show elevated Nb/Yb ratios (Fig. 11a, b, c). This is most evident in magma M1, which may be perceived as being derived from melt-enriched mantle, i.e. mantle rocks enriched in incompatible elements (HFSE and REE) that are only mobile in melts (e.g. Pearce & Peate, 1995). Magma M2, on the other hand, is mainly enriched in fluid-mobile incompatible elements (LILE), reflecting an additional subduction-related slab component.

The composition of the mafic dykes was thus controlled by mixing of these magma/source components (mostly seen in immobile incompatible

https://doi.org/10.1017/S0016756813000551 Published online by Cambridge University Press

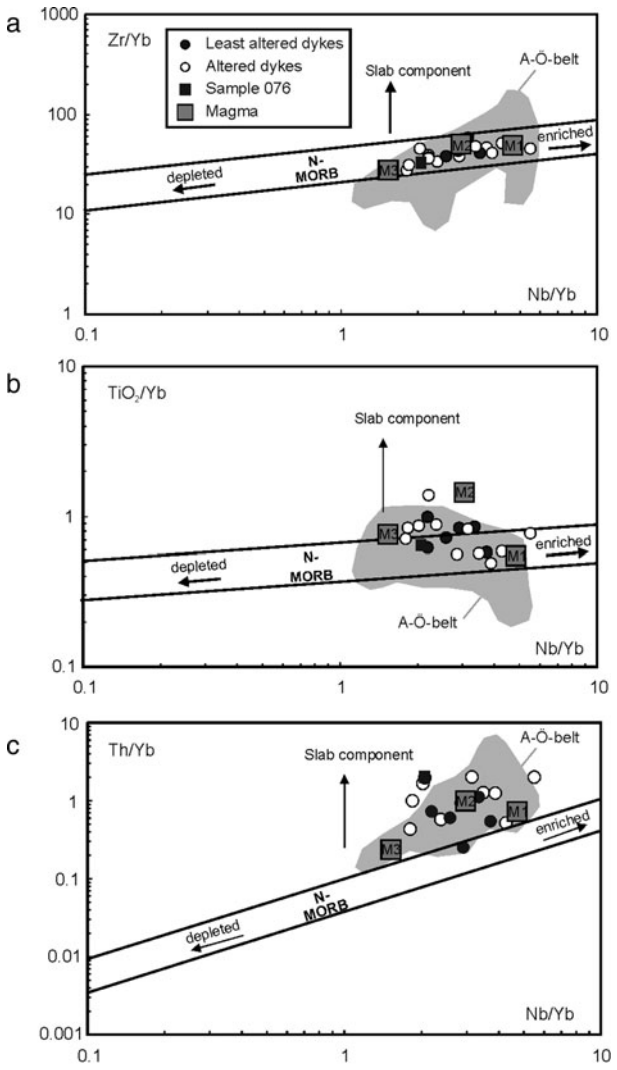

Figure 11. (a) Zr/Yb; (b) TiO_2/Yb and (c) Th/Yb versus Nb/Yb (after Pearce & Peate, 1995), suggesting an enriched MORB source with an additional slab component visible for Ti and Th. M1–M3 are the inferred end-member magma compositions. Grey shaded areas show the composition of gabbros and diorites from the Avesta–Östhammar belt (Johansson & Hålenius, 2013).

elements and Nd isotopes), supplemented by various degrees of fractionation (affecting the compatible elements more strongly). It is not known exactly when and where the mixing and fractionation process outlined above occurred. Mixing may have occurred already in the source, such that distinct mantle sources generated individual magmas defined within the compositional space of the end-member magmas, or by mixing of magmas of the distinct end-member magma compositions. Regardless of process (or combination of the processes), the mantle magmas rose, mixed and fractionated in several magma chambers to arrive at the final unique compositions of each emplaced dyke. The combined mixing and fractionation processes were then overprinted by metasomatic alteration, particularly depletion in Na_2O and enrichment in K_2O and Rb.

5.d Tectonic setting

All of the Dannemora dyke samples have a sub-alkalic basalt composition (Fig. 12a). The characteristic shape of the trace element variation diagram (Figs 7b, 10b), with enrichment in LILE and LREE and relative depletion in Nb–Ta and Zr–Hf, suggests that the Dannemora dykes formed from mafic magmatism in a subduction-related environment (e.g. Pearce & Peate, 1995; Davidson, 1996). The 'LILE hump', most marked in magma M2 (Fig. 10b), is therefore partly related to subduction enrichment of the source although it has probably been enhanced by metasomatic additions to some of the samples.

The calc-alkaline character and the tectonic setting in an active continental margin (ACM) are consistent in most of the tectonic discrimination diagrams (Fig. 12b, c, d). In the ternary Th-Hf-Ta diagram (Fig. 12b) the samples cluster along a line oriented approximately perpendicular to the Th corner. Part of the scatter in Th may however be caused by alteration. This spread in Th is also noticeable in the Th/Yb versus Ta/Yb plot (Fig. 12d), which classifies about 2/3 of the samples as within plate volcanic zone (WPVZ). As the Bergslagen region is interpreted as a back-arc (Allen *et al.* 1996), the WPVZ signature might have emanated from the upwelling of enriched mantle below thinned continental crust, perhaps during initial back-arc extension. The ratio between subduction zone component and MORB component can change over time (Pearce & Peate, 1995) and the influence of the subduction zone component decreases when the back-arc region 'matures' into back-arc spreading (Pearce *et al.* 1981). However, the relatively rare occurrence of basaltic rocks in the Bergslagen region suggests that the extension ceased before back-arc spreading was fully developed into sea-floor spreading.

In summary, similarly to the Herräng dykes, the Dannemora dykes are inferred to have intruded into already-formed continental crust during an extensional event (possibly related to back-arc spreading) rather than in a primitive island-arc during active subduction. The island arc or subduction signature seen in several of the diagrams may be inherited from a source previously affected by subduction, and need not necessarily indicate an island-arc environment or ongoing subduction at the time of dyke intrusion.

5.e Source character

Partial melting of the mantle results in a residue depleted in incompatible elements. The HFSE in Figures 7b and 10b show similar or lower contents than MORB, pointing towards an early depletion event in the mantle source of the Dannemora dykes. As stated earlier, the great variation of, for example, Nb and Zr is ascribed to heterogeneities within the mantle source region giving rise to at least three different source magmas, followed by fractionation and magma mixing, rather than contamination from upper continental crust or alteration. Heterogeneities with variable

https://doi.org/10.1017/S0016756813000551 Published online by Cambridge University Press

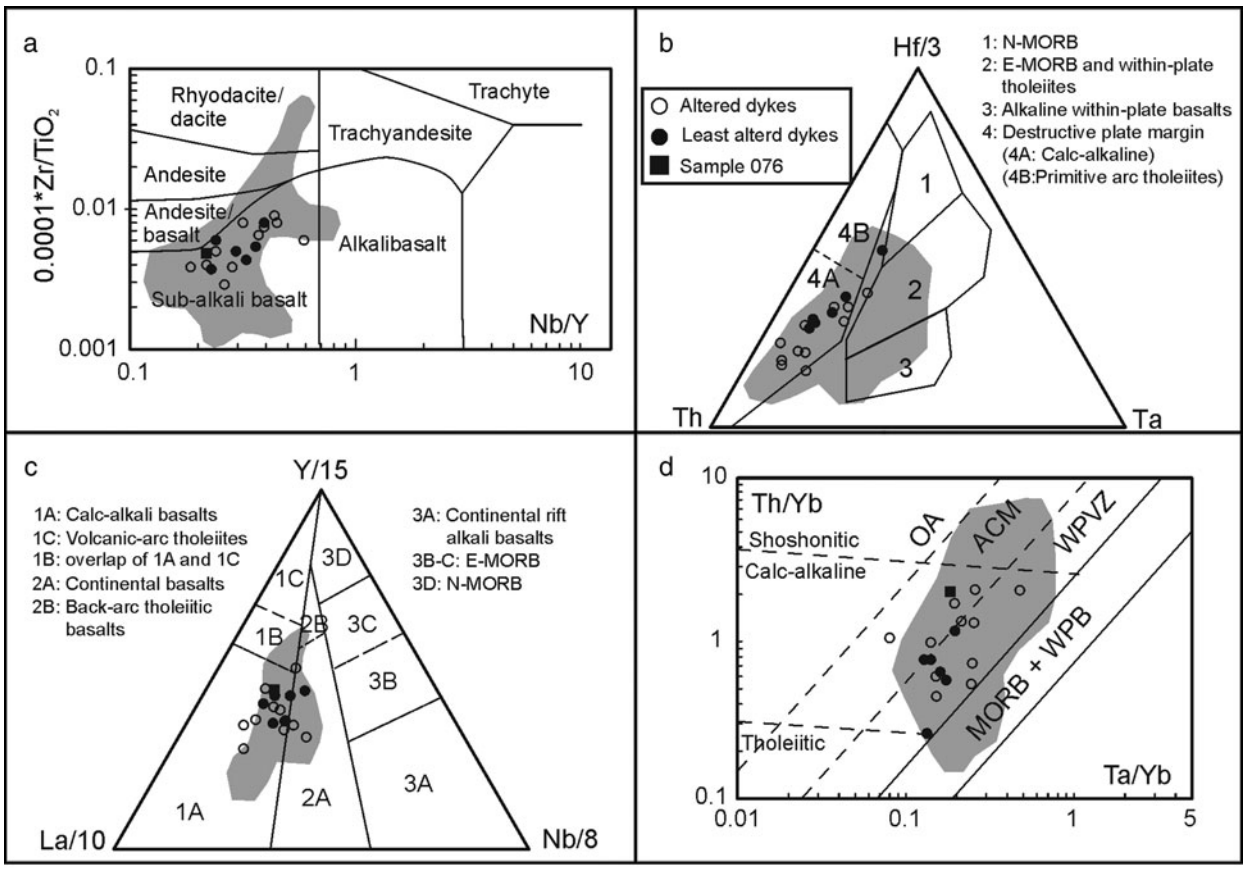

Figure 12. Tectonic discrimination diagrams. Sample 076 is marked with a filled square. (a) Zr/TiO_2 versus Nb/Y, where the rocks plot as sub-alkaline basalts (after Winchester & Floyd, 1977). (b) Th-Hf-Ta diagram, where the rocks classify as calc-alkaline derived from subduction-related magmas (after Wood, 1980). (c) The calc-alkaline and active continental margin character of the rocks is also supported by the La-Y-Nb diagram (after Cabanis & Lecolle, 1989). (d) Th/Yb versus Ta/Yb plot, showing a vertical scatter between active continental margin (ACM) and within-plate volcanic zone (WPVZ). OA – oceanic arc; WPB – within plate basalt; MORB – mid-ocean ridge basalt (after Pearce, 1983; Gorton & Schandl, 2000). Grey shaded areas show composition of gabbros and diorites from the Avesta–Östhammar belt (Johansson & Hålenius, 2013).

re-enrichment of incompatible elements may have developed during subduction-related magmatism at *c.* 1.9 Ga, or even prior to that. The enriched character of the source regions may be explained by the additions of LILE, Th, U and LREE by fluids and melts released from the subducting slab by dewatering and melting of sediments and hydrothermally altered oceanic crust (e.g. Pearce & Peate, 1995). Partial melting of such re-enriched mantle sections generated the LILE- and LREE-enriched Dannemora dyke magmas. Similar models were advocated for 1.9–1.8 Ga basic rocks from elsewhere in the Swedish Svecofennian and TIB by e.g. Andersson (1997*b*), Andersson *et al.* (2004*a*, 2006*b*, 2007, 2011), Johansson *et al.* (2012) and Johansson & Hålenius (2013).

The elevated Nb/Yb ratios also point to an enriched MORB-like source, with magma M1 being more enriched than magma M2 and M3 (Fig. 11a, b, c; after Pearce & Peate, 1995). An additional subduction-related slab component is not visible for Zr (Fig. 11a), but partly for TiO_2 (Fig. 11b) and clearly for Th (Fig. 11c). Andersson (1997*b*), Andersson *et al.* (2004*a*, 2006*b*, 2007, 2011), Rutanen & Andersson (2009), Andersen *et al.* (2009) and Rutanen *et al.* (2011) concluded that the Palaeoproterozoic sub-Svecofennian mantle in the central part of the Fennoscandian shield was heterogeneous and 'mildly depleted' (i.e. enriched after depletion). Since the Dannemora dykes probably formed some time after the intrusion of the Roslagen gabbro cumulates (Johansson *et al.* 2012) and the Avesta–Östhammar gabbros and diorites (Johansson & Hålenius, 2013), heterogeneities within the sub-continental mantle would have had even more possibilities to develop. Scatter between the ACM and WPVZ in Figure 12d might also by explained by a heterogeneous source region.

Figure 8 shows a plot of initial ε_{Nd} versus initial ε_{Sr} at 1870 Ma together with data on other basic rocks in the same region from Johansson *et al.* (2012) and Johansson & Hålenius (2013). The Dannemora dykes show similar isotopic character as the Roslagen gabbro cumulates and the Avesta–Östhammar gabbros and diorites with mildly depleted initial ε_{Nd} and enriched initial ε_{Sr}, and with sample 076 falling within the same range. However, compared to the Roslagen gabbro cumulates and Avesta–Östhammar mafic rocks, the Dannemora rocks spread in their initial ε_{Sr} values to considerably

https://doi.org/10.1017/S0016756813000551 Published online by Cambridge University Press

higher values. This spread is not correlated with the degree of metasomatic alteration. Metasomatism mainly involved the addition of K and Rb (cf. Figs 5, 6) and would therefore result in an increase of the Rb/Sr ratio. If this occurred significantly after the time of crystallization it would result in shifts of the initial ε_{Sr} to lower values, often below the mantle evolution curve. However, as the ε_{Sr} values extend consistently to higher values this must reflect either true magmatic compositions or the addition of radiogenic Sr at some later time.

6 Summary and conclusions

1. The Dannemora mafic dykes probably belong to the same dyke swarm as the E–W-trending Herräng dykes and coeval dykes at Forsmark dated to between 1870 and 1860 Ma. They intruded the supracrustal sequence at Dannemora as well as surrounding synmagmatic granitoids (GDG suite), and were later deformed and metamorphosed to greenschist facies.

2. The analysed dyke samples have basaltic composition, with SiO_2 between 46 and 51 wt %, MgO between 5 and 11 wt %, and Mg number between 47 and 71.

3. The dykes carry a mixed signature of subduction and within-plate volcanic zone magmatism and probably formed during an extensional phase of the Svecofennian orogeny, possibly related to initial back-arc spreading. The subduction signature may be inherited from mantle source rocks previously modified by subduction-related magmatism.

4. Their initial $^{87}Sr/^{86}Sr$ ratios and ε_{Sr} values show substantial spread to high values, possibly affected by post-crystallization modifications of the Rb–Sr system. Their initial ε_{Nd} values fall within a narrow range between +0.4 and +1.6, indicating a 'mildly depleted' mantle source with respect to Nd.

5. A combination of trace element and isotope geochemistry suggests that these dykes formed from a mixture of at least three different mantle-derived basaltic magma components, representing variably enriched sources with different degrees of enrichment in incompatible trace elements. The concentrations of incompatible trace elements in the dykes were mainly controlled by mixing between these components with limited influence from fractionation, whereas the MgO, Cr, Ni and Co concentrations were strongly controlled by fractionation of basaltic magma.

6. The three inferred magma components are broadly similar in composition to the inferred start magmas for the Roslagen gabbro cumulates and the Avesta–Östhammar belt gabbros and diorites, and to the trace and rare earth element pattern of volcanic arc basalts in general.

Acknowledgements. Thanks to Karin Wallner who helped with the isotope laboratory work and to Hans Schöberg who processed the isotope data. Abigail Barker and Karin Högdahl of Uppsala University are thanked for valuable discussions and input. Dannemora Mineral AB and the Geological Survey of Sweden (SGU) are acknowledged for economic support to this project. Reviews by Tom Andersen, Oslo and one anonymous reviewer substantially improved the paper.

References

ALLEN, R. L., LUNDSTRÖM, I., RIPA, M., SIMEONOV, A. & CHRISTOFFERSON, H. 1996. Facies analysis of a 1.9 Ga, continental marin, back-arc, felsic caldera province with diverse Zn-Pb-Ag (Cu-Au) sulfide and Fe oxide deposits, Bergslagen Region, Sweden. *Economic Geology* **91**, 979–1008.

ANDERSEN, T., ANDERSSON, U. B., GRAHAM, S., ÅBERG, G. & SIMONSEN, S. L. 2009. Granitic magmatism by melting of juvenile continental crust: New constraints on the source of Palaeoproterozoic granitoids in Fennoscandia from Hf isotopes in zircon. *Journal of the Geological Society, London* **166**, 233–47.

ANDERSSON, U. B. 1991. Granitoid episodes and mafic-felsic magma interaction in the Svecofennian of the Fennoscandian Shield, with main emphasis on the ~1.8 Ga plutonics. In *Precambrian Granitoids: Petrogenesis, Geochemistry and Metallogeny* (eds I. Haapala & K. C. Condie), pp. 127–139. *Precambrian Research* **51**.

ANDERSSON, U. B. 1997*a*. The sub-Jotnian Strömsbro rapakivi complex at Gävle, Sweden. *GFF* **119**, 159–67.

ANDERSSON, U. B. 1997*b*. Petrogenesis of some Proterozoic granitoid suites and associated basic rocks in Sweden (geochemistry and isotope geology). Sveriges Geologiska Undersökning, Rapporter och Meddelanden, **91**, 216 pp.

ANDERSSON, U. B. 2005. Age and P-T paths of metamorphism in the Bergslagen region, southern Sweden. *SGU-rapport* 2005-7, 22–4.

ANDERSSON, U. B., BEGG, G. C., GRIFFIN, W. L. & HÖGDAHL, K. 2011. Ancient and juvenile components in the continental crust and mantle: Hf isotopes in zircon from Svecofennian magmatic rocks and rapakivi granites in Sweden. *Lithosphere* **3**, 409–19.

ANDERSSON, U. B., EKLUND, O. & CLAESON, D. T. 2004*a*. Geochemical character of the mafic-hybrid magmatism in the Småland-Värmland belt. *Geological Survey of Finland, Special Paper* **37**, 47–55.

ANDERSSON, U. B., HÖGDAHL, K., SJÖSTRÖM, H. & BERGMAN, S. 2006*a*. Multistage growth and reworking of the Palaeoproterozoic crust in the Bergslagen area, southern Sweden: evidence from U-Pb geochronology. *Geological Magazine* **143**, 679–97.

ANDERSSON, U. B., EKLUND, O., FRÖJDÖ, S. & KONOPELKO, D. 2006*b*. 1.8 Ga magmatism in the Fennoscandian shield; lateral variations in subcontinental mantle enrichment. *Lithos* **86**, 110–36.

ANDERSSON, U. B., RUTANEN, H., JOHANSSON, Å., MANSFELD, J. & RIMŠA, A. 2007. Characterization of the Paleoproterozoic mantle beneath the Fennoscandian Shield: Geochemistry and isotope geology (Nd, Sr) of ~1.8 Ga mafic plutonic rocks from the Transscandinavian Igneous Belt in Southeast Sweden. *International Geology Review* **49**, 587–625.

ANDERSSON, U. B., SJÖSTRÖM, H., HÖGDAHL, K. & EKLUND, O. 2004*b*. The Transscandinavian Igneous belt, evolutionary models. *Geological Survey of Finland, Special Paper* **37**, 104–12.

https://doi.org/10.1017/S0016756813000551 Published online by Cambridge University Press

BEUNK, F. F. & KUIPERS, G. 2012. The Bergslagen ore province, Sweden: Review and update of an accreted orocline, 1.9–1.8 Ga BP. *Precambrian Research* **216–19**, 95–119.

CABANIS, B. & LECOLLE, M. 1989. Le diagramme La/10-Y/15-Nb/8. Un outil pour la discrimination des séries volcaniques et la mise en évidence des processus de mélange et/ou de contamination crustale. *Comptes Rendus de l'Academie des Sciences Serie II*, **309**, 2023–29.

DAHLIN, P., ALLEN, R. & SJÖSTRÖM, H. 2012. Palaeoproterozoic metavolcanic and metasedimentary succession hosting the Dannemora iron ore deposits, Bergslagen region, Sweden. *GFF* **134**, 71–85.

DAVIDSON, J. 1996. Deciphering mantle and crustal signatures in subduction zone magmatism. *Geophysical Monograph* **98**, 251–62.

DE PAOLO, D. J. 1981. Neodymium isotopes in the Colorado Front Range and crust-mantle evolution in the Proterozoic. *Nature* **291**, 193–96.

DICKIN, A. 1995. *Radiogenic Isotope Geology*. Cambridge: Cambridge University Press, 452 pp.

GAÁL, G. & GORBATSCHEV, R. 1987. An outline of the Precambrian evolution of the Baltic shield. *Precambrian Research* **35**, 15–52.

GORTON, M. & SCHANDL, E. S. 2000. From continents to island arcs: a geochemical index of tectonic setting for arc-related and within-plate felsic to intermediate volcanic rocks. *The Canadian Mineralogist* **38**, 1065–73.

HASTIE, A. R., KERR, A. C., PEARCE, J. A. & MITCHELL, S. F. 2007. Classification of altered volcanic island arc rocks using immobile trace elements: development of the Th-Co discrimination diagram. *Journal of Petrology* **48**, 2341–57.

HERMANSSON, T., STEPHENS, M. B., CORFU, F., ANDERSSON, J. & PAGE, L. 2007. Penetrative ductile deformation and amphibolite-facies metamorphism prior to 1851 Ma in the western part of the Svecofennian orogen, Fennoscandian Shield. *Precambrian Research* **153**, 29–45.

HERMANSSON, T., STEPHENS, M. B., CORFU, F., PAGE, L. M. & ANDERSSON, J. 2008. Migratory tectonic switching, western Svecofennian orogen, central Sweden. Constraints from U/Pb zircon and titanite geochronology. *Precambrian Research* **161**, 250–78.

HÖGDAHL, K., ANDERSSON, U. B. & EKLUND, O. (eds) 2004. The Transscandinavian Igneous Belt (TIB) in Sweden: a review of its character and evolution. *Geological Survey of Finland, Special Paper* **37**, 125 pp.

HÖGDAHL, K., SJÖSTRÖM, H. & BERGMAN, S. 2009. Ductile shear zones related to crustal shortening and domain boundary evolution in the central Fennoscandian Shield. *Tectonics* **28**, TC1003, doi:10.1029/2008TC002277.

HUGHES, C. J. 1972. Spilites, keratophyres, and the igneous spectrum. *Geological Magazine* **109**, 513–27.

ISHIZUKA, O., YUASA, M., TAMURA, Y., SHUKUNO, H., STERN, R. J., NAKA, J., JOSHIMA, M. & TAYLOR, R. N. 2010. Migrating shoshonitic magmatism tracks Izu–Bonin–Mariana intra-oceanic arc rift propagation. *Earth and Planetary Science Letters* **294**, 111–22.

JACOBSEN, S. B. & WASSERBURG, G. J. 1984. Sm-Nd isotopic evolution of chondrites and achondrites. *II. Earth and Planetary Science Letters* **67**, 137–50.

JOHANSSON, Å., ANDERSSON, U. B. & HÅLENIUS, U. 2012. Petrogenesis and geotectonic setting of early Svecofennian arc cumulates in the Roslagen area, east-central Sweden. *Geological Journal* **47**, 557–93.

JOHANSSON, Å. & HÅLENIUS, U. 2013. Palaeoproterozoic mafic intrusions along the Avesta-Östhammar belt, east-central Sweden: mineralogy, geochemistry and magmatic evolution. *International Geology Review* **55**, 131–57.

KELEMEN, P. B., HANGHØJ, K. & GREENE, A. R. 2005. One view of the geochemistry of subduction-related magmatic arcs, with an emphasis on primitive andesite and lower crust. In *The Crust* (ed. R. L. Rudnick), pp. 593–659. Amsterdam: Elsevier, Treatise on Geochemistry no. 3.

KORJA, A. K., LAHTINEN, R. & NIRONEN, M. 2006. The Svecofennian orogen: a collage of microcontinents and island arcs. In *European Lithosphere Dynamics* (eds D. G. Gee & R. A. Stephenson), pp. 561–78. Geological Society of London, Memoirs no. 32.

LAGER, I. 2001. The geology of the Palaeoproterozoic limestone-hosted Dannemora iron deposit, Sweden. Sveriges Geologiska Undersökning: Rapporter och Meddelanden **107**, 49 pp.

LAHTINEN, R., KORJA, A. & NIRONEN, M. 2005. Palaeoproterozoic tectonic evolution of the Fennoscandian Shield. In *The Precambrian Bedrock of Finland: Key to the Evolution of the Fennoscandian Shield* (eds M. Lehtinen, P. Nurmi & O. T. Rämö), 418–532. Amsterdam: Elsevier.

LESLIE, R. A. J., DANYUSHEVSKY, L. V., CRAWFORD, A. J. & VERBEETEN, A. C. 2009. Primitive shoshonites from Fiji: Geochemistry and source components. *Geochemistry Geophysics Geosystems* **10**, Q07001, doi:10.1029/2008GC002326.

LUNDSTRÖM, I., ALLEN, R. L., PERSSON, P.-O. & RIPA, M. 1998. Stratigraphies and depositional ages of Svecofennian, Palaeoproterozoic meta-volcanic rocks in E. Svealand and Bergslagen, south central Sweden. *GFF* **120**, 315–20.

MACLEAN, W. H. & BARRETT, T. J. 1993. Lithogeochemical techniques using immobile elements. *Journal of Geochemical Exploration* **48**, 109–33.

MAGNUSSON, N. H. 1940. Herrängsfältet och dess järnmalmer. Sveriges Geologiska Undersökning C 431, 78 pp (in Swedish).

MCCULLOCH, M. T. & CHAPPELL, B. W. 1982. Nd isotopic characteristics of S- and I-type granites. *Earth and Planetary Science Letters* **58**, 51–64.

MEEN, J. K. 1987. Formation of shoshonites from calc-alkaline basalt magmas: geochemical and experimental constraints from the type locality. *Contributions to Mineralogy and Petrolology* **97**, 333–51.

MILLER, C., SCHUSTER, R., KLÖTZLI, U., FRANK, W. & PURTSCHELLER, F. 1999. Post-collisional potassic and ultrapotassic magmatism in SW Tibet; geochemical and Sr-Nd-Pb-O isotopic constraints for mantle source characteristics and petrogenesis. *Journal of Petrology* **40**, 1399–424.

NESBITT, H. W. & YOUNG, G. M. 1984. Prediction of some weathering trends of plutonic and volcanic rocks based upon thermodynamic and kinematic considerations. *Geochimica Cosmochimica Acta* **48**, 1523–34.

NESBITT, H. W. & YOUNG, G. M. 1989. Formation and diagenesis of weathering profiles. *The Journal of Geology* **97**, 129–47.

NIRONEN, M. 1997. The Svecofennian orogen: a tectonic model. *Precambrian Research* **86**, 21–44.

OEN, I. S., HELMERS, H., VERSCHURE, B. H. & WIKLANDER, U. 1982. Ore deposition in a Proterozoic incipient rift zone environment. A tentative model for the Filipstad-Grythyttan-Hjulsjö region, Bergslagen Sweden. *Geologische Rundschau* **71**, 182–94.

https://doi.org/10.1017/S0016756813000551 Published online by Cambridge University Press

PEARCE, J. A. 1983. Role of the sub-continental lithosphere in magma genesis at active continental margins. In *Continental Basalts and Mantle Xenoliths* (eds C. Hawkesworth J. & M. J. Norry), 230–49. Nantwich, UK: Shiva Geology Series.

PEARCE, J. A., ALABASTER, T., SHELTON, A. W. & SEARLE, M. 1981. The Oman Ophiolite as a Cretaceous arc-basin complex. Evidence and implications. *Philosophical Transactions of the Royal Society of London Series A: Mathematical Physical and Engineering Sciences* **300**, 299–317.

PEARCE, J. A. & PEATE, D. W. 1995. Tectonic implications of the composition of volcanic arc magmas. *Annual Review of Earth and Planetary Sciences* **23**, 251–85.

PE-PIPER, G. 1983. Triassic shoshonites and andesites, Lakmon Mountains, western continental Greece: Differences in primary geochemistry and sheet silicate alteration products. *Lithos* **16**, 23–33.

PERSSON, K. S. & SJÖSTRÖM, H. 2003. Late-orogenic progressive shearing in eastern Bergslagen, central Sweden. *GFF* **125**, 23–36.

PIN, C. & ZALDUEGUI, J. F. S. 1997. Sequential separation of light rare-earth elements, thorium and uranium by miniaturized extraction chromatography. Application to isotopic analyses of silicate rocks. *Analytica Chimica Acta* **339**, 79–89.

RISKU-NORJA, H. 1992. Geochemistry of the dolerite dykes in Södermanland, eastern central Sweden. *GFF* **114**, 67–91.

RUTANEN, H. & ANDERSON, U. B. 2009. Mafic plutonic rocks in a continental-arc setting: geochemistry of 1.87–1.78 Ga rocks from south-central Sweden and models of their Palaeotectonic setting. *Geological Journal* **44**, 241–79.

RUTANEN, H., ANDERSSON, U. B., VÄISÄNEN, M., JOHANSSON, Å., FRÖJDÖ, S., LAHAYE, Y. & EKLUND, O. 2011. 1.8 Ga magmatism in southern Finland: strongly enriched mantle and juvenile crustal sources in a post-collisional setting. *International Geology Review* **53**, 1622–83.

SÖDERLUND, U., ISACHSEN, C. E., BYLUND, G., HEAMAN, L. M., PATCHETT, P. J., VERVOORT, J. D. & ANDERSSON, U. B. 2005. U–Pb baddeleyite ages and Hf, Nd isotope chemistry constraining repeated mafic magmatism in the Fennoscandian Shield from 1.6 to 0.9 Ga. *Contributions to Mineralogy and Petrology* **150**, 174–94.

STÅLHÖS, G. 1991. Beskrivning till berggrundskartorna Östhammar NV, NO, SV, SO med sammanfattande översikt av basiska gångar, metamorfos och tektonik i östra Mellansverige. Sveriges Geologiska Undersökning Af 161, 166, 169, 172, Uppsala. 249 pp (in Swedish).

STEPHENS, M. B., AHL, M., BERGMAN, T., LUNDSTRÖM, I., PERSSON, L., RIPA, M. & WAHLGREN, C.-H. 2007. Regional geological and geophysical maps of Bergslagen and surrounding areas. Bedrock map. Sveriges Geologiska Undersökning Ba 58.1, Uppsala.

STEPHENS, M. B., AHL, M., BERGMAN, T., LUNDSTRÖM, I., PERSSON, L., RIPA, M. & WAHLGREN, C. H. 2009. Synthesis of the bedrock geology in the Bergslagen region, Fennoscandian Shield, south-central Sweden. Sveriges Geologiska Undersökning Ba 58, Uppsala, 259 pp.

STURCHIO, N. C., MUEHLENBACHS, K. & SEITZ, M. G. 1986. Element redistribution during hydrothermal alteration of rhyolite in an active geothermal system - Yellowstone drill cores Y-7 and Y-8. *Geochimica et Cosmochimica Acta* **50**, 1619–31.

SUN, S. S. & MCDONOUGH, W. F. 1989. Chemical and isotopic systematics of oceanic basalts. Implications for mantle composition and processes. In *Magmatism in Ocean Basins* (eds A. D. Saunders & M. J. Norry), 313–45. Geological Society of London, Special Publication no. 42.

TIRÉN, S. A. & BECKHOLMEN, M. 1990. Influence of regional shear zones on the lithological pattern in central Sweden. *GFF* **112**, 197–9.

TÖRNEBOHM, A. E. 1878. *Beskrifning till Geologisk Atlas öfver Dannemora Grufvor*. Beckman, Stockholm, 85 pp (in Swedish).

TURNER, S., ARNAUD, N., LIU, J., ROGERS, N., HAWKESWORTH, C., HARRIS, N., KELLEY, S., VAN CALSTEREN, P. & DENG, Q. 1996. Post-collision, shoshonitic volcanism on the Tibetan plateau: implication for convective thinning of the lithosphere and source of ocean island basalts. *Journal of Petrology* **37**, 45–71.

VAN DER VELDEN, W., BAKER, J., DE MAESSCHALCK, S. & VAN MEERTEN, T. 1982. Bimodal volcanism in the Grythytte Field and associated volcano-plutonic complexes, Bergslagen, Central Sweden. *Geologische Rundschau* **71**, 171–81.

WIKSTRÖM, A. 1992. Some composite dikes in Sweden. *GFF* **114**, 385–94.

WINCHESTER, J. A. & FLOYD, P. A. 1977. Geochemical discrimination of different magma series and their different products using immobile element. *Chemical Geology* **20**, 325–43.

WOOD, D. A. 1980. The application of a Th-Hf-Ta diagram to problems of tectonomagmatic classification and to establishing the nature of crustal contamination of basaltic lavas of the British Tertiary volcanic province. *Earth and Planetary Science Letters* **50**, 11–30.

YANG, W.-B., NIU, H.-C., SHAN, Q., LUO, Y., SUN, W.-D., LI, C.-Y., LI, N.-B., & YU, X.-Y. 2012. Late Paleozoic calc-alkaline to shoshonitic magmatism and its geodynamic implications, Yuximolegai area, western Tianshan, Xinjiang. *Gondwana Research* **22**, 325–40.

ZHANG, Z., XIAO, X., WANG, J., WANG, Y. & KUSKY, T. M. 2008. Post-collisional Plio-Pleistocene shoshonitic volcanism in the western Kunlun Mountains, NW China: Geochemical constraints on mantle source characteristics and petrogenesis. *Journal of Asian Earth Sciences* **31**, 379–403.

ZHAO, Z., MO, X., DILEK, Y., NIU, Y., DE PAOLO, D. J., ROBINSON, P., ZHU, D., SUN, C., DONG, G., ZHOU, S., LUO, Z. & HOU, Z. 2009. Geochemical and Sr-Nd-Pb-O isotopic compositions of the post-collisional ultrapotassic magmatism in SW Tibet: petrogenesis and implications for India intra-continental subduction beneath southern Tibet. *Lithos* **113**, 190–212.

https://doi.org/10.1017/S0016756813000551 Published online by Cambridge University Press